FEMTOSECOND OPTICAL PARAMETRIC OSCILLATORS BASED ON POTASSIUM TITANYL PHOSPHATE CRYSTALS

A THESIS

SUBMITTED TO THE DEPARTMENT OF ELECTRICAL AND ELECTRONICS ENGINEERING

AND THE INSTITUTE OF ENGINEERING AND SCIENCES

OF BILKENT UNIVERSITY

IN PARTIAL FULFILLMENT OF THE REQUIREMENTS

FOR THE DEGREE OF

MASTER OF SCIENCE

By

Tolga Kartaloğlu

September 1996

FEMTOSECOND OPTICAL PARAMETRIC OSCILLATORS BASED ON POTASSIUM TITANYL PHOSPHATE CRYSTALS

A THESIS

SUBMITTED TO THE DEPARTMENT OF ELECTRICAL AND

ELECTRONICS ENGINEERING

AND THE INSTITUTE OF ENGINEERING AND SCIENCES

OF BILKENT UNIVERSITY

IN PARTIAL FULFILLMENT OF THE REQUIREMENTS

FOR THE DEGREE OF

MASTER OF SCIENCE

Tolga Kartaloğlu.

By

Tolga Kartaloğlu

September 1996

I certify that I have read this thesis and that in my opinion it is fully adequate, in scope and in quality, as a thesis for the degree of Master of Science.

Assist. Prof. Dr. Orhan Aytür (Supervisor)

I certify that I have read this thesis and that in my opinion it is fully adequate, in scope and in quality, as a thesis for the degree of Master of Science.

Prof. Dr. Ayhan Altıntaş

I certify that I have read this thesis and that in my opinion it is fully adequate, in scope and in quality, as a thesis for the degree of Master of Science.

Assist. Prof. Dr. Ekmel Özbay

Approved for the Institute of Engineering and Sciences:

Prof. Dr. Mehmet Baray
Director of Institute of Engineering and Sciences

ABSTRACT

FEMTOSECOND OPTICAL PARAMETRIC OSCILLATORS BASED ON POTASSIUM TITANYL PHOSPHATE CRYSTALS

Tolga Kartaloğlu
M.S. in Electrical and Electronics Engineering
Supervisor: Assist. Prof. Dr. Orhan Aytür
September 1996

In this thesis, we describe our experiments to construct and characterize optical parametric oscillators (OPO) based on a potassium titanyl phosphate (KTP) crystals. The oscillator is synchronously pumped by a mode-locked Titanium:Sapphire laser at a wavelength of 745 nm, a pulse duration of 120 fs, and average power of 640 mW. The OPO converts the 745 nm pump beam to a signal beam at 1068 nm. The resonator is in the form of a ring cavity, with the KTP crystal positioned at the intracavity focus. The crystal is cut for type-II phase matching. We investigated the performance of the OPO with four different output coupler reflectivities. The 10% output coupler gives the best results with 170 mW of signal average power, corresponding to 27% conversion efficiency. The signal beam has an autocorrelation pulse width of 650 fs. In addition, we demonstrate phase-matched intracavity frequency doubling of the signal beam with the same KTP crystal, by placing a waveplate inside the resonator. The waveplate is used to rotate the polarization for type-II phase matching.

Keywords: optical parametric oscillation, self-doubling OPO, nonlinear crystals, KTP, intracavity second harmonic generation, ultrafast lasers, femtosecond, Ti:Sapphire.

ÖZET

POTASYUM TİTANİL FOSFAT KRİSTALİ TEMELLİ FEMTOSANİYE OPTİK PARAMETRİK OSİLATÖRLER

Tolga Kartaloğlu
Elektrik ve Elektronik Mühendisliği Bölümü Yüksek Lisans
Tez Yöneticisi: Yar. Doç. Dr. Orhan Aytür
Eylül 1996

Bu tez, potasyum titanil fosfat (KTP) kristali bazlı optik parametrik osilatörler (OPO) kurmak ve değerlendirmek için yaptığımız deneyleri anlatmaktadır. Dalgaboyu 745 nm, darbe uzunluğu 120 fs, ve ortalama gücü 640 mW olan bir Titanyum:Safir lazeri ile osilatörü senkronize olarak pompaladık. OPO, 745 nm dalgaboyundaki pompa ışınını 1068 nm dalgaboyundaki sinyal ışınına çevirdi. KTP kristalini bir halka resonatörün resonatör-içi odağına koyduk. Kristal tip-II faz uyumu için kesilmişti. Dört değişik yansıtma oranlı çıkış aynası ile OPO'nun performansını inceledik. %10'luk çıkış aynası, %27 lik dönüştürme verimine karşılık gelen, 170 mW ortalama gücüyle en iyi sonucu verdi. Sinyal ışını 650 fs otokorelasyon darbe uzunluğundaydı. Ayrıca, resonatör içine dalga geciktirici koyarak, aynı KTP kristalinde faz uyumlu, resanatör içi sinyal ışınının frekans katlanmasını gösterdik. Dalga geciktirici, tip-II faz uyumu için sinyal polarizasyonunu çevirmekte kullanıldı.

Anahtar kelimeler: optik parametrik osilator, kendiliğinden katlamalı OPO, doğrusal olmayan kristaller, KTP, kovuk içi ikinci harmonik üretimi, ultra hızlı lazerler, femtosaniye, Titanyum:Safir.

ACKNOWLEDGEMENTS

I would like to thank Dr. Orhan Aytür for his supervision, special guidance, suggestion, and especially encouragement through the development of this thesis.

I am grateful to Kahraman Güçlü Köprülü for his help during the development of the thesis and experimental work.

I would also like to express my thanks to the Turkish Scientific and Technical Research Council and NATO for their partial support of this work under Grant No. EEEAG-118 and Grant No. TU-MIMIC, respectively.

TABLE OF CONTENTS

LIST OF FIGURES

Chapter 1

Introduction

Ever since the invention of the laser by Maiman [1] in 1960, there has been a great deal of interest in the development of continuously tunable coherent sources. Such laser sources have broad applications in both research and industry. The development of such tunable lasers is difficult, since lasers operate at discrete wavelengths due to their nature of light generation with stimulated emission between quantized energy levels. Only when these quantized levels form a continuous bands of energy, a laser can be continuously tunable. Even then, the tuning range is quite limited. Therefore, converting the frequency of a laser beam to another frequency in a tunable way is an important task.

The first example of frequency conversion was frequency doubling of a ruby laser using a quartz crystal by Fraken [2] in 1965. Due to the nonlinear response of the crystal, a light beam at the twice the frequency (second harmonic) of the laser beam was generated. This up-conversion process was of course not tunable.

There are many kinds of lasers operating at different frequencies. They produce pulsed or continuous wave beams with different characteristics. Two laser beams of different frequencies also nonlinearly interact with each other resulting in a beam at the sum or difference frequencies. Again, the generated frequencies have discrete values. Also, there are synchronization problems for the pulsed lasers; and also various beam characteristics may not match, resulting in further difficulties.

Second harmonic, sum and difference frequency generation are three-photon optical parametric processes. In the sum frequency generation process, two

photons at different frequencies are combined to produce a photon at the sum frequency. Second harmonic generation (SHG) is the special case in which the frequency of the two photons are same. The difference frequency generation process can be thought of as the reverse process of sum frequency generation in which one photon is split into two photons at lower frequencies.

Optical parametric oscillators (OPO) are truly tunable sources of coherent radiation. They are similar to lasers in that an optical resonator is used to provide feedback to a gain medium. However, they use material nonlinearities as the gain medium, where the virtual energy levels involved are tunable. As a result, very broad continuous tuning of frequency can be achieved. OPOs are optically pumped and generate beams of frequencies lower than the pump frequency. With the simultaneous use of SHG with OPO, we can obtain frequencies both above and below the pump frequency.

The first proposal and theory of optical parametric oscillator were due to Kroll [3] in 1962, and the first demonstration of optical parametric oscillation is by Giordmaine and Miller [4] in 1965. The main idea is the use of the spontaneous parametric process. In the spontaneous parametric process, a photon at frequency ω_p breaks down into signal and idler photons at lower frequencies ω_s and ω_i, respectively. In this process, energy and momentum are conserved, that is $\omega_p = \omega_s + \omega_i$ and $\mathbf{k_p} = \mathbf{k_s} + \mathbf{k_i}$. The spontaneous parametric process, followed by repeated difference frequency generations, leads to a parametric amplification of the signal light. An optical parametric oscillator can be constructed by simply adding optical feedback, just as in a laser.

An OPO is analogous to the optically pumped three-level laser. The frequency of the pump beam determines the top energy level. The mid energy level can be tuned through momentum conservation, which is called the phase matching condition. By changing material properties affecting the propagation of the light beams, the phase matching condition is satisfied for different frequencies. Therefore, frequency conversion to any desired frequency can be achieved.

There have been many demonstrations of optical parametric oscillators [5] with different kind of lasers as the pump source. A continuous wave pumped OPO generates continuous wave output. The cavity sizes can be as small as the length of nonlinear crystal. Generally, continuous wave lasers are not suitable for OPO application, because nonlinear processes are more efficient at high intensities. Q-switched lasers provide pulses with pulse widths in the order of 10 ns and high peak powers with low repetition rates. Pulsed OPOs pumped

by such lasers can be very efficient. A new oscillation starts with each pulse.

Although the ultrafast laser systems have pulsed outputs, their operation characteristic are similar to continuous wave lasers. The short duration of ultrafast pump pulses (on the order of 100 fs) clearly implies that synchronous pumping must be used. This means that the pump pulse propagates in synchronism with the signal pulse in the nonlinear crystal and always meets the signal pulse as it travels back and forth in the cavity.

The first femtosecond OPO was pumped by a Rhodamine 6G dye laser [6]. Since that time, there have been many demonstrations of Titanium:Sapphire (Ti:Sapphire) laser pumped femtosecond OPOs around 100 MHz repetition rate with less than 150 fs pulse widths.

A Ti:sapphire laser produces nearly chirp-free pulses with pulse widths around 100 fs with repetition rates in the order of 100 MHz. It is a tunable laser with a wavelength range between 700 and 1000 nm. With the second harmonic generation process, the wavelength range can be extended from 350 to 500 nm. By using an OPO, the wavelength range can be extended above the 1000 nm. The upper limit determined by the transparency of the todays nonlinear crystals is around 4 μm. With the SHG of the OPO output, the frequency gap between the output and the second harmonic of the Ti:Sapphire can also be covered, extending the continuous tunability range from 0.35 μm to 4 μm.

In this thesis, we designed and implemented synchronously pumped femtosecond optical parametric oscillators based on potassium titanyl phosphate (KTP) crystals. We used a mode-locked Titanium:Sapphire laser as our pump source. In addition, we demonstrate phase-matched intracavity frequency doubling of the signal beam with the same KTP crystal when a halfwave plate is placed inside the resonator.

In Chapter 2, the theoretical background for nonlinear media and optical parametric amplification and oscillation are given. Chapter 3 describes the experimental setup and our measurements. In this chapter, we also discuss the results. Remarks and conclusions are provided in Chapter 4.

Chapter 2

Theory of Optical Parametric Amplifiers and Oscillators

In this chapter, we start with a description of nonlinear materials and discuss the interaction of three light waves through a quadratic nonlinearity. To describe three wave mixing, we derive three coupled wave equations starting from Maxwell's equations. The general solution and parametric amplification as a special solution are given next. Finally, optical parametric oscillators are discussed.

2.1 Nonlinear Materials

Nonlinear behavior of materials was observed shortly after the invention of laser [2]. High optical intensities of lasers enable us to observe nonlinear behavior of materials. A variety of materials show large nonlinearities. Three wave mixing is the interaction of three light waves at different frequencies in a material showing a quadratic type nonlinearity. Second harmonic, sum frequency and difference frequency generation are examples of three wave mixing process.

In nonlinear materials, we assume that we can represent the total electric field $\mathbf{E}(\mathbf{r}, t)$ of the optical waves that interact with each other as a discrete sum

of a number of frequency components as

$$\mathbf{E}(\mathbf{r},t) = \sum_i \mathrm{Re}(\mathbf{E_i}(\mathbf{r})e^{j\omega_i t}) = \frac{1}{2}\sum_i (\mathbf{E_i}(\mathbf{r})e^{j\omega_i t} + \mathbf{E_i^*}(\mathbf{r})e^{-j\omega_i t}) \tag{2.1}$$

where $\mathbf{E_i}(\mathbf{r})$ is the slowly varying electric field phasor at angular frequency ω_i. As the light wave propagates through the material, it induces a polarization field $\mathbf{P}(\mathbf{r},t)$. The polarization field can also be written in terms of a sum of a number of frequency components as

$$\mathbf{P}(\mathbf{r},t) = \sum_i \mathrm{Re}(\mathbf{P_i}(\mathbf{r})e^{j\omega_i t}) = \frac{1}{2}\sum_i (\mathbf{P_i}(\mathbf{r})e^{j\omega_i t} + \mathbf{P_i^*}(\mathbf{r})e^{-j\omega_i t}). \tag{2.2}$$

Again, $\mathbf{P}(\mathbf{r})$ is the slowly varying polarization field phasor at angular frequency ω_i. The general relation between the polarization and the electric fields is nonlinear and dispersive [7]. A nonlinear dependence of polarization can be expressed as a power series of the electric field in time domain. Dispersion, being a property that states frequency dependence, can be expressed as a multiplicative function in the frequency domain. When we write the polarization field in time domain, this multiplicative function becomes a convolution. Also, all of the coefficients of the power series are tensors, because the materials involved are anisotropic. The relation between $\mathbf{P}(\mathbf{r},t)$ and $\mathbf{E}(\mathbf{r},t)$ can be given as

$$\begin{aligned}\mathbf{P}(\mathbf{r},t) = \epsilon_0 \int_{-\infty}^{t} \overline{\overline{\chi}}^{(1)}(t-t')\cdot\mathbf{E}(\mathbf{r},t')dt' + \\ \epsilon_0 \int_{-\infty}^{t}\int_{-\infty}^{t} \overline{\overline{\overline{\chi}}}^{(2)}(t-t',t-t'') : \mathbf{E}(\mathbf{r},t')\mathbf{E}(\mathbf{r},t'')dt'dt'' + \text{h.o.t.}\end{aligned} \tag{2.3}$$

where ϵ_0 is the permittivity of free space, and $\overline{\overline{\chi}}^{(1)}$ is the linear susceptibility tensor of second rank, and $\overline{\overline{\overline{\chi}}}^{(2)}$ is the second-order nonlinear susceptibility tensor of third rank. Each element of the tensor is first convolved with the components of the electric field and then summed over the corresponding indices. In this representation, the first term,

$$\mathbf{P}(\mathbf{r},t) = \epsilon_0 \int_{-\infty}^{t} \overline{\overline{\chi}}^{(1)}(t-t')\cdot\mathbf{E}(\mathbf{r},t')dt' \tag{2.4}$$

is the linear polarization. The next term,

$$\mathbf{P}(\mathbf{r},t) = \epsilon_0 \int_{-\infty}^{t}\int_{-\infty}^{t} \overline{\overline{\overline{\chi}}}^{(2)}(t-t',t-t'') : \mathbf{E}(\mathbf{r},t')\mathbf{E}(\mathbf{r},t'')dt'dt'', \tag{2.5}$$

is the second-order nonlinear polarization term. In this term, the second order susceptibility tensor relates two electric fields to the polarization field. Also,

higher order terms (h.o.t.) that are smaller compared to the second-order term exist. Those terms are effective in centrosymmetric materials that have a center of inversion symmetry. In such materials, the second-order nonlinear susceptibility tensor vanishes. In the case of our experiment, we have nonzero $\overline{\overline{\chi}}^{(2)}$ and can neglect all higher order terms.

Two electric fields at frequencies ω_2 and ω_1 give rise to a nonlinear polarization phasor at angular frequency $\omega_3 = \omega_2 + \omega_1$ as

$$\begin{aligned} \mathbf{P}_3^{(2)}(\mathbf{r}) &= \frac{1}{2}\epsilon_0\overline{\overline{\chi}}^{(2)}(\omega_3 = \omega_1 + \omega_2) : \mathbf{E_1}(\mathbf{r})\mathbf{E_2}(\mathbf{r}) \\ &\quad + \frac{1}{2}\epsilon_0\overline{\overline{\chi}}^{(2)}(\omega_3 = \omega_2 + \omega_1) : \mathbf{E_2}(\mathbf{r})\mathbf{E_1}(\mathbf{r}). \end{aligned} \tag{2.6}$$

Since, $\mathbf{E_1}(\mathbf{r})$ and $\mathbf{E_2}(\mathbf{r})$ are associated with time dependences $e^{j\omega_1 t}$ and $e^{j\omega_2 t}$, respectively, the second-order nonlinear polarization resulting from their product is at the sum frequency. Therefore, $\overline{\overline{\chi}}^{(2)}$ can be expressed as a function of three frequencies for which one of them is always related to the other two by sum or difference. Full permutation symmetry property and Kleinman's symmetry condition [7] state that we can write

$$\overline{\overline{\chi}}^{(2)}(\omega_3 = \omega_1 + \omega_2) = \overline{\overline{\chi}}^{(2)}(\omega_3 = \omega_2 + \omega_1). \tag{2.7}$$

Then, the second-order nonlinear polarization term takes form

$$\mathbf{P}_3^{(2)}(\mathbf{r}) = \epsilon_0\overline{\overline{\chi}}^{(2)}(\omega_3 = \omega_1 + \omega_2) : \mathbf{E_1}(\mathbf{r})\mathbf{E_2}(\mathbf{r}). \tag{2.8}$$

The important fact is that although we do not have an electric field at frequency ω_3, we have a polarization at frequency ω_3. This induced time-varying polarization acts as a source of electromagnetic radiation at frequency ω_3.

Similarly,

$$\mathbf{P}_1^{(2)}(\mathbf{r}) = \epsilon_0\overline{\overline{\chi}}^{(2)}(\omega_1 = \omega_3 - \omega_2) : \mathbf{E_3}(\mathbf{r})\mathbf{E_2^*}(\mathbf{r}) \tag{2.9}$$

$$\mathbf{P}_2^{(2)}(\mathbf{r}) = \epsilon_0\overline{\overline{\chi}}^{(2)}(\omega_2 = \omega_3 - \omega_1) : \mathbf{E_3}(\mathbf{r})\mathbf{E_1^*}(\mathbf{r}) \tag{2.10}$$

can be written. Equations (2.8), (2.9), and (2.10) show that there is a coupling between three fields at ω_1, ω_2, and $\omega_3 = \omega_1 + \omega_2$ through the second-order nonlinearity.

2.2 Coupled Wave Equations

A set of equations can be used to describe the second-order nonlinear interactions of three light waves. They are derived from Maxwell's equations for a

source free, and lossless medium,

$$\nabla \times \mathbf{E} = -\frac{\partial \mathbf{B}}{\partial t} \tag{2.11}$$

$$\nabla \times \mathbf{H} = -\frac{\partial \mathbf{D}}{\partial t} \tag{2.12}$$

$$\nabla \cdot \mathbf{D} = 0 \tag{2.13}$$

$$\nabla \cdot \mathbf{B} = 0 \tag{2.14}$$

and constitutive relations for a magnetically isotropic and inactive medium,

$$\begin{aligned} \mathbf{D} &= \epsilon_0 \mathbf{E} + \mathbf{P} \\ \mathbf{B} &= \mu_0 \mathbf{H}. \end{aligned} \tag{2.15}$$

where ϵ_0 and μ_0 are the permittivity and the permeability of free space, $\mathbf{E}$ and $\mathbf{H}$ are the electric and magnetic fields, $\mathbf{D}$ and $\mathbf{B}$ are the electric and magnetic flux densities, and $\mathbf{P}$ is the induced polarization, respectively. The constitutive relation between the electric field and the electric flux density takes the form of

$$\begin{aligned} \mathbf{D_L} &= \epsilon_0 \mathbf{E} + \mathbf{P^{(1)}} \\ &= \epsilon_0 \overline{\overline{\epsilon}}_\mathbf{r} \cdot \mathbf{E} \end{aligned} \tag{2.16}$$

$$\mathbf{D} = \mathbf{D_L} + \mathbf{P^{(2)}}, \tag{2.17}$$

when we separate the linear and nonlinear parts of the polarization field, where $\mathbf{D_L}$ denotes the linear part of electric flux density and $\overline{\overline{\epsilon}}_\mathbf{r}$ is the relative permeability tensor defined as

$$\overline{\overline{\epsilon}}_\mathbf{r} = \overline{\overline{1}} + \overline{\overline{\chi}}^{(1)}. \tag{2.18}$$

where $\overline{\overline{1}}$ is a three by three identity matrix.

Just as the homogeneous wave equation [8], the nonlinear driven wave equation

$$\nabla \times \nabla \times \mathbf{E}(\mathbf{r},t) + \mu_0 \frac{\partial^2}{\partial t^2} \mathbf{D_L}(\mathbf{r},t) = -\mu_0 \frac{\partial^2}{\partial t^2} \mathbf{P^{(2)}}(\mathbf{r},t) \tag{2.19}$$

is derived by taking curl of Equation (2.11) and using Equation (2.12). When the right hand side of Equation (2.19) is zero, it become the homogeneous linear wave equation.

Nonlinear interactions occur over distances and times that are much larger than the individual sinusoidal variation of the optical field. Therefore, a plane wave representation with slowly varying envelope functions can be used. For

light waves at frequencies ω_1, ω_2, and $\omega_3 = \omega_2 + \omega_1$ propagating along the z direction, we can write the electric and polarization phasors as

$$\mathbf{E_i}(\mathbf{r}) = \hat{\mathbf{a}}_\mathbf{i} A_i(z) e^{-jk_i z} \tag{2.20}$$

$$\mathbf{P_i^{(2)}}(\mathbf{r}) = \hat{\mathbf{a}}_\mathbf{i} B_i(z) e^{-jk_i' z} \tag{2.21}$$

where $i = 1, 2, 3$. The unit vector $\hat{\mathbf{a}}_\mathbf{i}$ represents the direction of polarization, $A_i(z)$ and $B_i(z)$ represent the slowly varying envelope functions of the electric field and the second-order nonlinear polarization field, and k_i and k_i' are the propagation constants of the electric field and polarization.

Most nonlinear materials are optically anisotropic, and hence exhibit birefringence. Birefringence is the dependence of the refractive index on the direction of the polarization of the optical radiation so that, for a given direction of propagation, there are two eigen-polarization directions corresponding to two eigen-refractive indices. We take these eigen-polarization directions to be x and y directions of our coordinate system. Then, the relative permeability tensor $\overline{\overline{\epsilon}}_\mathbf{r}$ is diagonalized in our new frame with the diagonal elements being the square of the eigen-refractive indices. The unit vector $\hat{\mathbf{a}}_\mathbf{i}$ is either $\hat{\mathbf{x}}$ or $\hat{\mathbf{y}}$. Note that, this new coordinate system is a linear but not orthogonal coordinate system; the plane wave propagation equations are now just like in the isotropic medium, a scalar refractive index is used. Details of propagation in an anisotropic medium can be found in Appendix A.

Relations between the slowly varying envelope functions $A_i(z)$ and $B_i(z)$ and between the propagation constants k_i and k_i' are found using Equations (2.8), (2.9), and (2.10) as

$$B_1(z) = \epsilon_0 d_1 A_3(\mathbf{r}) A_2^*(\mathbf{r}) \tag{2.22}$$

$$B_2(z) = \epsilon_0 d_2 A_3(\mathbf{r}) A_1^*(\mathbf{r}) \tag{2.23}$$

$$B_3(z) = \epsilon_0 d_3 A_1(\mathbf{r}) A_2(\mathbf{r}) \tag{2.24}$$

$$k_1' = k_3 - k_2 \tag{2.25}$$

$$k_2' = k_3 - k_1 \tag{2.26}$$

$$k_3' = k_1 + k_2 \tag{2.27}$$

where

$$d_1 = \frac{1}{2}\hat{\mathbf{a}}_\mathbf{1} \cdot \overline{\overline{\overline{\chi}}}^{(\mathbf{2})}(\omega_1 = \omega_3 - \omega_2) : \hat{\mathbf{a}}_\mathbf{3}\hat{\mathbf{a}}_\mathbf{2} \tag{2.28}$$

$$d_2 = \frac{1}{2}\hat{\mathbf{a}}_\mathbf{2} \cdot \overline{\overline{\overline{\chi}}}^{(\mathbf{2})}(\omega_2 = \omega_3 - \omega_1) : \hat{\mathbf{a}}_\mathbf{3}\hat{\mathbf{a}}_\mathbf{1} \tag{2.29}$$

$$d_3 = \frac{1}{2}\hat{\mathbf{a}}_3 \cdot \overline{\overline{\chi}}^{(2)}(\omega_3 = \omega_1 + \omega_2) : \hat{\mathbf{a}}_1\hat{\mathbf{a}}_2 \tag{2.30}$$

are the effective second-order nonlinear coefficients. In a lossless medium, due to full permutation symmetry [7], all three effective nonlinear coefficients are equal and can be represented by a single real coefficient

$$d_{\text{eff}} = d_1 = d_2 = d_3. \tag{2.31}$$

With the above definition of the electric field, polarization, and effective nonlinear coefficient, the nonlinear driven wave equation can be expressed in frequency domain as

$$\begin{aligned} &\nabla \times \nabla \times \left(A_i(z)e^{-jk_i z}\right)\hat{\mathbf{a}}_\mathbf{i} \\ &\quad -\mu_0\epsilon_0\omega_i^2\overline{\overline{\epsilon}}_\mathbf{r} \cdot \hat{\mathbf{a}}_\mathbf{i}A_i(z)e^{-jk_i z} = \mu_0\omega_i^2\hat{\mathbf{a}}_\mathbf{i}B_i(z)e^{-jk_i' z} \end{aligned} \tag{2.32}$$

Note that

$$\overline{\overline{\epsilon}}_\mathbf{r} \cdot \hat{\mathbf{a}}_\mathbf{i} = n_i^2\hat{\mathbf{a}}_\mathbf{i}. \tag{2.33}$$

Since we have

$$\nabla \cdot \mathbf{E} = \nabla \cdot \left(A_i(z)e^{-jk_i z}\hat{\mathbf{a}}_\mathbf{i}\right) = 0 \tag{2.34}$$

We can use the vector identity, $\nabla \times \nabla \times \mathbf{E} = \nabla(\nabla \cdot \mathbf{E}) - \nabla^2\mathbf{E} = -\nabla^2\mathbf{E}$, and the wave equation takes the form

$$\left[\nabla^2\left(A_i(z)e^{-jk_i z}\right) + \mu_0\epsilon_0 n_i^2\omega_i^2 A_i(z)e^{-jk_i z}\right] = -\mu_0\omega_i^2 B_i(z)e^{-jk_i' z}. \tag{2.35}$$

With the slowly varying envelope representation, we get three coupled equations for the envelope functions

$$\frac{d^2A_1(z)}{dz^2} - 2jk_1\frac{dA_1(z)}{dz} = -\mu_0\epsilon_0\omega_1^2 d_{\text{eff}}A_3(z)A_2^*(z)e^{-j\Delta kz} \tag{2.36}$$

$$\frac{d^2A_2(z)}{dz^2} - 2jk_2\frac{dA_2(z)}{dz} = -\mu_0\epsilon_0\omega_2^2 d_{\text{eff}}A_3(z)A_1^*(z)e^{-j\Delta kz} \tag{2.37}$$

$$\frac{d^2A_3(z)}{dz^2} - 2jk_3\frac{dA_3(z)}{dz} = -\mu_0\epsilon_0\omega_3^2 d_{\text{eff}}A_1(z)A_2(z)e^{j\Delta kz}. \tag{2.38}$$

where

$$\Delta k = k_3 - k_2 - k_1 \tag{2.39}$$

is called the phase mismatch.

We can neglect the second-order z derivatives under the slowly varying envelope approximation,

$$\left|\frac{d^2A_i(z)}{dz^2}\right| \ll \left|k_i\frac{dA_i(z)}{dz}\right| \tag{2.40}$$

and the coupled equations take the form

$$\frac{dA_1(z)}{dz} = -j\frac{\omega_1 d_{\text{eff}}}{cn_1}A_3(z)A_2^*(z)e^{-j\Delta kz} \tag{2.41}$$

$$\frac{dA_2(z)}{dz} = -j\frac{\omega_2 d_{\text{eff}}}{cn_2}A_3(z)A_1^*(z)e^{-j\Delta kz} \tag{2.42}$$

$$\frac{dA_3(z)}{dz} = -j\frac{\omega_3 d_{\text{eff}}}{cn_3}A_1(z)A_2(z)e^{j\Delta kz}. \tag{2.43}$$

where

$$c = \frac{1}{\sqrt{\epsilon_0\mu_0}}. \tag{2.44}$$

is the speed of light waves in free space. Equation (2.41) through (2.43) describe the evolution of the slowly varying envelopes in three wave mixing.

2.3 Phase Matching

When we consider the coupled wave equations (Equations (2.41), (2.41), and (2.43)), there are two important quantities in all the equations. These quantities are important because they determine the strength of the nonlinear interaction. One of these quantities is the effective nonlinear coefficient d_{eff}; larger values make the interaction stronger. The other quantity is the phase mismatch Δk. The term $e^{j\Delta kz}$ has unity magnitude, but it effects the phase of the interaction. With advance in distance, it can change the sign of the fields and reverse the interaction. For the effectiveness of the interaction, the phase matching condition

$$\Delta k = 0 \tag{2.45}$$

must be satisfied [7]. The phase mismatch depends on the direction of propagation. For a given nonlinear material and interaction frequencies, Δk can vanish for certain directions of propagation inside the nonlinear material.

We can re-write the phase matching condition

$$k_3 - k_2 - k_1 = 0 \tag{2.46}$$

in terms of the angular frequencies and the refractive indices seen by each light wave as

$$\omega_3 n_3 - \omega_2 n_2 - \omega_1 n_1 = 0. \tag{2.47}$$

Using the frequency relation $\omega_3 = \omega_2 + \omega_1$ a reduced equation between the angular frequencies and refractive indices can be obtained as

$$\omega_2(n_3 - n_2) + \omega_1(n_3 - n_1) = 0 \tag{2.48}$$

The refractive index of a material is a function of frequency due to dispersion. There are two characteristic behaviors of refractive index for optical materials. It is either monotonically increasing or decreasing with the frequency. For both cases, the above equation cannot be satisfied, since both terms have the same sign and the sum cannot vanish. However, many materials display birefringence, so that there are two refractive indices depending on the polarization of the optical field. As a result, we can satisfy the phase matching condition for a given set of frequencies at a certain propagation direction by using different polarization directions for the interacting light waves. The details of anisotropic materials and phase matching can be found in Appendices A and B.

2.4 Optical Parametric Amplification

The general solution of the coupled mode equations are given in terms of Jacobi elliptic functions [9]. This section outlines these solutions. We assume that the interaction begins at $z = 0$ and ends at $z = L$. The envelope functions can be written in polar form,

$$A_n(z) = \rho_n e^{j\phi_n}. \tag{2.49}$$

The phase angle for the interaction is defined as

$$\theta = \Delta k + \phi_3 - \phi_1 - \phi_2. \tag{2.50}$$

By defining the total intensity as

$$I = I_1(0) + I_2(0) + I_3(0) \tag{2.51}$$

the envelope functions can be normalized using

$$u_n(z) = \sqrt{\frac{I_n(z)}{\omega_n I}}. \tag{2.52}$$

The normalized distance

$$\xi = \frac{d_{\text{eff}}(2\omega_1\omega_2\omega_3 I)^{1/2}}{(\epsilon_0 c_0^3 n_1 n_2 n_3)^{1/2}} z \tag{2.53}$$

and the normalized phase mismatch

$$\Delta S = \frac{\Delta k z}{\xi} = \frac{(\epsilon_0 c_0^3 n_1 n_2 n_3)^{1/2}}{d_{\text{eff}}(2\omega_1\omega_2\omega_3 I)^{1/2}} \Delta k \tag{2.54}$$

are also defined. A parameter that depends on the initial values of the normalized lengths and the phase is given as

$$\Gamma = u_1(0)u_2(0)u_3(0)\cos(\theta(0)) + \frac{1}{2}\Delta S u_3^2(0). \tag{2.55}$$

There are three invariants over the normalized length ξ defined as

$$m_1 = u_3^2 + u_1^2 \tag{2.56}$$

$$m_2 = u_3^2 + u_2^2 \tag{2.57}$$

$$m_3 = u_1^2 - u_2^2 \tag{2.58}$$

These invariants correspond to Manley-Rowe relations and represent the conservation of the number of photons for a lossless medium. With the roots u_{3a}^2, u_{3b}^2, and u_{3c}^2 of the cubic polynomial

$$u_3^2(m_1 - u_3^2)(m_2 - u_3^2) - (\Gamma - \frac{1}{2}\Delta S u_3^2)^2 = 0 \tag{2.59}$$

$$u_{3c}^2 \geq u_{3b}^2 \geq u_{3a}^2 \geq 0 \tag{2.60}$$

and substitutions

$$y^2 = (u_3^2 - u_{3a}^2)/(u_{3b}^2 - u_{3a}^2) \tag{2.61}$$

$$\gamma^2 = (u_{3b}^2 - u_{3a}^2)/(u_{3c}^2 - u_{3a}^2) \tag{2.62}$$

the solution to the normalized envelope functions are given as

$$y(\xi) = \mathrm{sn}((u_{3c}^2 - u_{3a}^2)^{1/2}(\xi + \xi_0), \gamma^2) \tag{2.63}$$

$$y(0) = \mathrm{sn}((u_{3c}^2 - u_{3a}^2)^{1/2}\xi_0, \gamma^2) \tag{2.64}$$

$$\xi_0 = \mathrm{F}(\arcsin(y(0)), \gamma^2)/(u_{3c}^2 - u_{3a}^2)^{1/2} \tag{2.65}$$

$$u_3^2(\xi) = u_{3a}^2 + (u_{3b}^2 - u_{3a}^2)y^2(\xi) \tag{2.66}$$

$$u_1^2(\xi) = m_1 - u_3^2(\xi) = u_1^2(0) + u_3^2(0) - u_3^2(\xi) \tag{2.67}$$

$$u_2^2(\xi) = m_2 - u_3^2(\xi) = u_2^2(0) + u_3^2(0) - u_3^2(\xi) \tag{2.68}$$

where $\mathrm{sn}(x, m)$ is the Jacobi elliptic function and $\mathrm{F}(\phi, m)$ is the elliptic integral of the first kind [10].

Optical parametric amplification is the process where two optical fields at frequencies ω_3 and ω_1 interact to produce light wave at the difference frequency $\omega_2 = \omega_3 - \omega_1$. In this process, a photon at frequency ω_3 is split into two photons at frequencies ω_1 and ω_2 resulting in an increase in the number of photons at frequency ω_1. The field at frequency ω_3 is called the pump, since it is the energy source for the newly created photons. The field at frequency ω_1 is called the signal, since it is the amplified field through the process, and the field at frequency ω_2 is called the idler.

We use the subscripts s, i and p instead of 1, 2 and 3 to represent the signal, idler, and pump fields. Figure 2.1 shows the schematic diagram of an

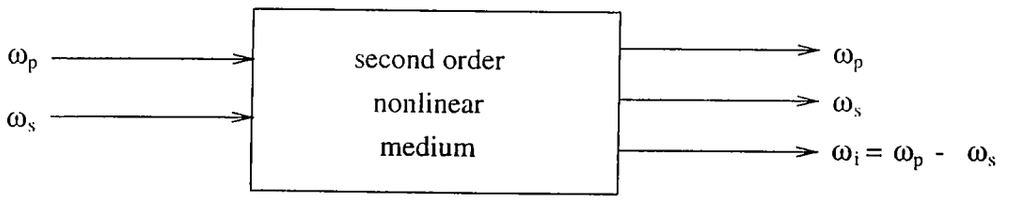

Figure 2.1: Schematic of an OPA.

optical parametric amplifier (OPA). With the initial conditions $I_p(0)$, $I_s(0)$, and $I_i(0) = 0$, and assuming perfect phase matching $\Delta k = 0$, we can find the evolution of the intensities of the pump, signal, and idler as they propagate in the nonlinear medium as

$$I_p(z) = I_p(0)\frac{1 - \mathrm{sn}^2(x,\gamma^2)}{1 - \gamma^2\,\mathrm{sn}^2(x,\gamma^2)} \tag{2.69}$$

$$I_s(z) = I_s(0) + I_s(0)\gamma^2\frac{\mathrm{sn}^2(x,\gamma^2)}{\mathrm{dn}^2(x,\gamma^2)} \tag{2.70}$$

$$I_i(z) = \frac{\omega_i}{\omega s}I_s(0)\gamma^2\frac{\mathrm{sn}^2(x,\gamma^2)}{\mathrm{dn}^2(x,\gamma^2)} \tag{2.71}$$

where

$$x = \frac{\kappa}{\gamma}z \tag{2.72}$$

$$\gamma^2 = \frac{1}{1 + \dfrac{\omega_p I_s(0)}{\omega_s I_p(0)}} \tag{2.73}$$

and κ defined to be

$$\kappa = \frac{d_{\mathrm{eff}}(2\omega_s\omega_i I_p(0))^{1/2}}{(\epsilon_0 c_0^3 n_s n_i n_p)^{1/2}} \tag{2.74}$$

and n_s, n_i, and n_p are the refractive indices of signal, idler, and pump fields, $\mathrm{sn}(x,m)$ and $\mathrm{dn}(x,m)$ are of the Jacobi elliptic functions. The intensities at the output of nonlinear medium can be calculated by using $z = L$ where L is the length of the nonlinear medium.

Figure 2.2 shows the evolution of the signal, idler, and pump photon fluxes as a function of normalized distance. The pump flux decreases as the signal and idler fluxes grow; at some distance, they reach a maximum where the pump is fully depleted. Then, back conversion starts, the idler and signal photons combine to generate pump photons, so the pump field begins to grow. In this plot, the photon flux of the signal input beam is taken to be 1% of the pump photon flux, as an example.

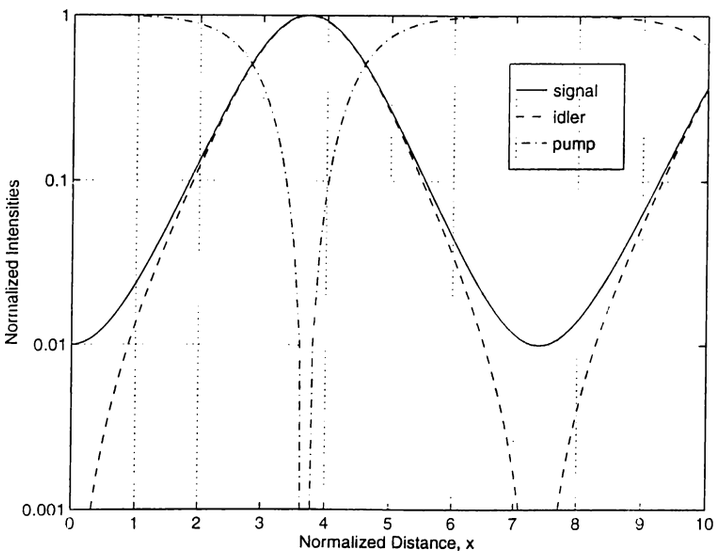

Figure 2.2: Evolution of the normalized intensities of the signal, idler, and pump beams as a function of the normalized distance for $\Delta k = 0$. The horizontal axis is the normalized distance x and the vertical axis is normalized intensities divided by the normalized initial intensity of the pump.

When we look for a limiting case in which the signal input is small

$$I_s \ll I_p \tag{2.75}$$

then the γ^2 value approaches unity

$$\gamma^2 \approx 1 \tag{2.76}$$

resulting in the Jacobi elliptic functions to be approximated as

$$\mathrm{sn}(x, \gamma^2) \approx \tanh(\kappa z) \tag{2.77}$$

$$\mathrm{dn}(x, \gamma^2) \approx \mathrm{sech}(\kappa z). \tag{2.78}$$

The intensities at the output of the nonlinear medium are calculated as

$$I_p(z = L) \approx I_p(0) \tag{2.79}$$

$$I_s(z = L) \approx I_s(0) + I_s(0) \sinh^2(\kappa z) = I_s(0) \cosh^2(\kappa z) \tag{2.80}$$

$$I_i(z = L) \approx \frac{\omega_i}{\omega_s} I_s(0) \sinh^2(\kappa z) \tag{2.81}$$

Those solutions are known as the undepleted pump solutions of the coupled mode equations in which the pump intensity is held constant.

Parametric gain is defined as

$$G = \frac{I_s(z = L)}{I_s(z = 0)} \tag{2.82}$$

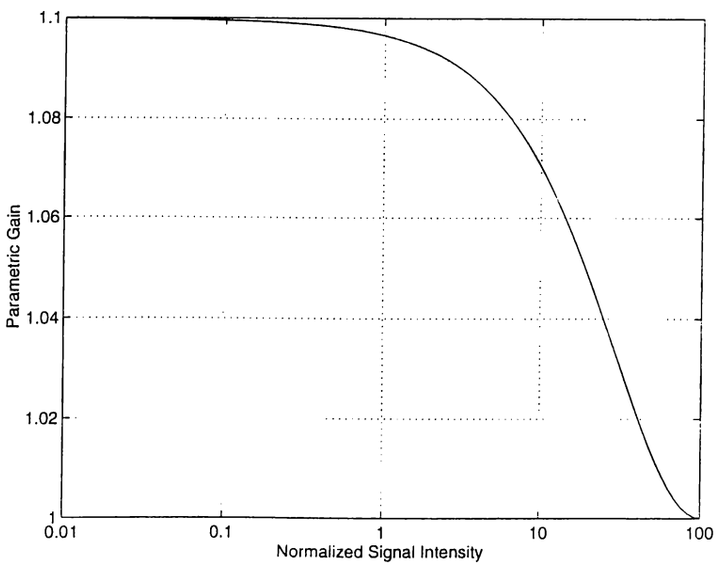

Figure 2.3: Gain saturation with the increase in signal input. The horizontal axis is the normalized signal intensity $u_s^2(0)$, the vertical axis is the gain.

and given by

$$G = 1 + \gamma^2 \frac{\mathrm{sn}^2(x, \gamma^2)}{\mathrm{dn}^2(x, \gamma^2)}. \tag{2.83}$$

Figure 2.3 shows the signal gain as a function of the ratio of the input signal intensity to the input pump intensity which is held constant. The argument x of the Jacobi elliptic functions is arbitrarily taken to be 0.311 so that the unsaturated gain is 1.1. The gain monotonically decreases to the limiting value of unity as the signal intensity increases. The gain at zero input is the small signal gain (unsaturated gain) and given as

$$G_0 = \cosh^2(\kappa z). \tag{2.84}$$

2.5 Optical Parametric Oscillators

The optical gain provided by a parametric amplifier can be used to make an optical oscillator with the help of a resonator. Such a device is known as an optical parametric oscillator (OPO). Figure 2.4 shows the schematic of an OPO. The signal field resonates inside a ring cavity formed by four mirrors. The output is obtained from a partially transmitting mirror called an output coupler (OC). All of the mirrors except the output coupler are high reflectors at the frequency of signal field. The pump field enters the cavity from one of the mirrors, which has special coatings that make it transparent to the pump

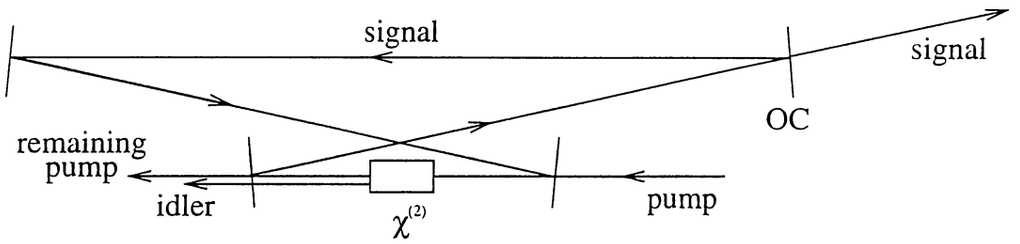

Figure 2.4: Schematic of an OPO.

wavelength, passes through gain medium and leaves cavity from other mirror. There is also an idler field which is generated in the nonlinear process. The mirrors are also transparent to idler beam, so that it does not resonate.

A simple model of an OPO is shown in Figure 2.5. The parametric amplifier is modeled as a gain medium where the gain saturates with increasing signal input as described by Equation (2.83). The output coupler has less than unity reflectance R_{OC}. The nonzero transmittance provides the output beam of the OPO. Unavoidable useless losses (less than unity reflectance of highly reflecting mirrors, losses in the nonlinear material, diffraction losses, etc...) are taken into account as a single source of loss which is represented by a lumped reflectance R_{L}. The total loss is defined to be

$$\alpha_T = 1 - R_{\mathrm{L}} R_{\mathrm{OC}}. \tag{2.85}$$

A cavity equation corresponding to steady state operation

$$G = \frac{1}{1 - \alpha_T} \tag{2.86}$$

can be written by equating round trip losses to the parametric gain. The OPO has a threshold. The pump intensity must exceed this threshold intensity I_{TH}. Figure 2.6 illustrates three possible situations. The dashed horizontal line represents the loss line which is equal to the inverse of the reflectances (right

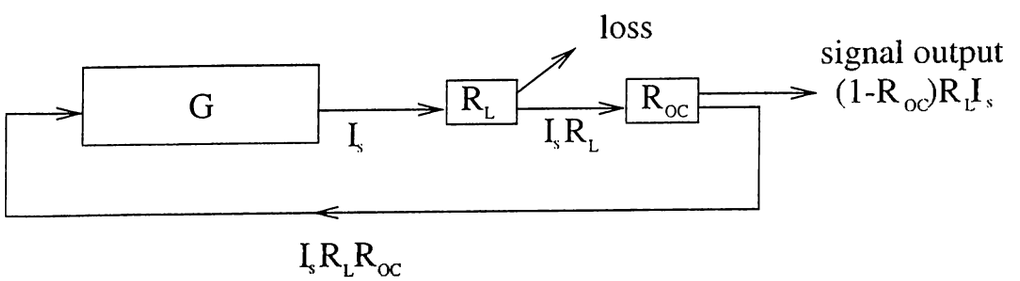

Figure 2.5: Model of OPO.

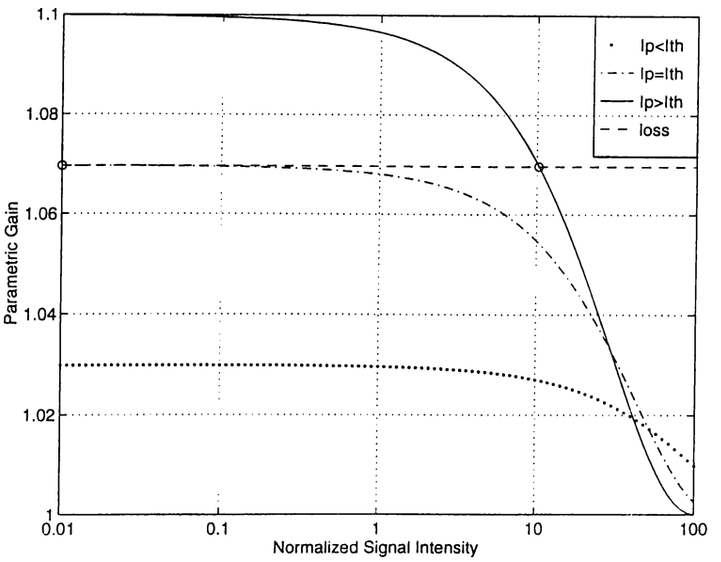

Figure 2.6: Gain curves for three different pump intensity. The horizontal axis is the normalized signal intensity $u_s^2(0)$, the vertical axis is the gain.

hand side of Equation (2.86)). Three gain curves corresponds to three pump intensities. The variables so selected that the argument x takes the values of 0.172, 0.262 , and 0.311. When input pump intensity is less than the threshold intensity ($I_p(0) < I_{\mathrm{TH}}$), the small signal gain is less than loss; as a result, there is no solution for the signal intensity inside the cavity resulting in the trivial solution

$$I_s = 0. \tag{2.87}$$

When the input pump intensity is equal to the threshold intensity ($I_p(0) = I_{\mathrm{TH}}$), the solution corresponds to

$$I_s = 0. \tag{2.88}$$

As a final case, when the input pump intensity is greater than the threshold intensity ($I_p(0) > I_{\mathrm{TH}}$), there is a solution with a nonzero signal field in side the cavity, represented by the intersection of the loss line with the gain curve.

At the threshold, the gain is just enough to compensate for the losses. Using the small signal gain equation (Equation (2.84)), the threshold pump intensity is found to be

$$I_{\mathrm{TH}} = \frac{\epsilon_0 c_0^3 n_s n_i n_p}{2 d_{\mathrm{eff}}^2 \omega_s \omega_i L^2} \left[\cosh^{-1}\left(\sqrt{\frac{1}{1-\alpha_T}}\right)\right]^2. \tag{2.89}$$

The threshold increases with increased loss (see Figure 2.7). We use typical numbers from our experiments (see Chapter 3) with $R_{\mathrm{OC}} = 0.93$ and $R_{\mathrm{L}} = 1$ to calculate the curves in Figure 2.7 through 2.10.

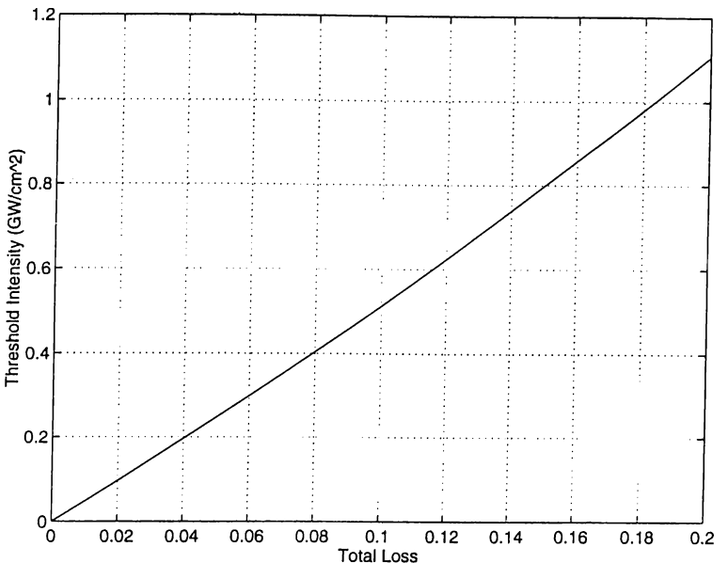

Figure 2.7: Threshold intensity as a function of total loss.

The signal output can be calculated using

$$I_o = (1 - R_{\mathrm{OC}})R_{\mathrm{L}}I_s \tag{2.90}$$

Figure 2.8 shows the output signal intensity as a function of pump intensity normalized to the threshold I_p/I_{TH}. The conversion efficiency is defined as

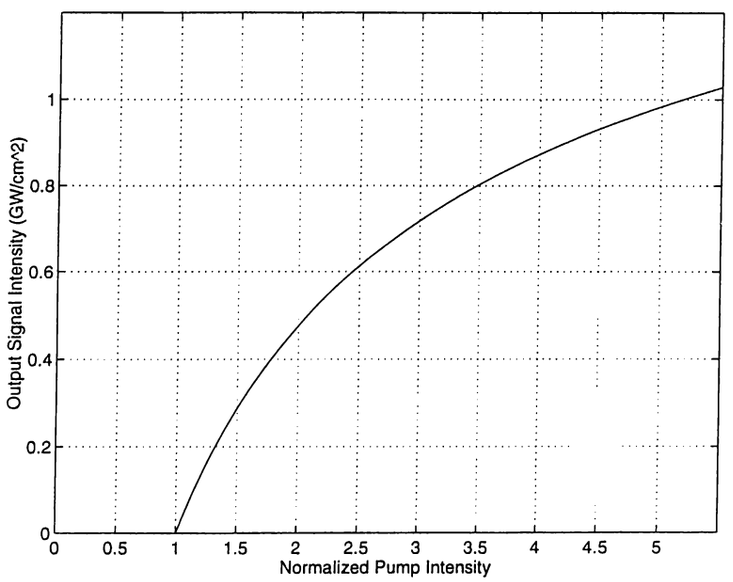

Figure 2.8: Output signal intensity as a function of pump intensity normalized to the threshold.

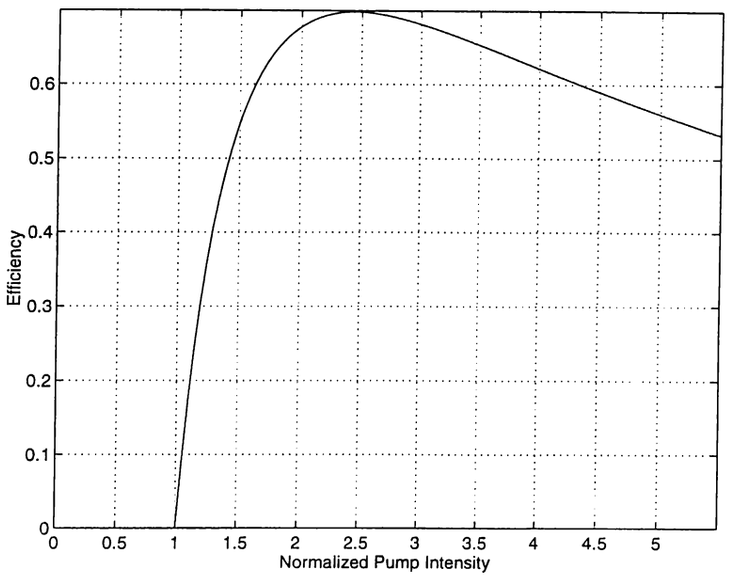

Figure 2.9: Conversion efficiency as a function of normalized pump intensity normalized to threshold.

$$\eta = \frac{I_o}{I_p} \tag{2.91}$$

Due to the photon energy ratio between the signal and pump the 100% intensity conversion efficiency cannot be observed. In Figure 2.9, the conversion efficiency is plotted as a function of pump intensity normalized to the threshold I_p/I_{TH}. The conversion efficiency has a maximum at a point where

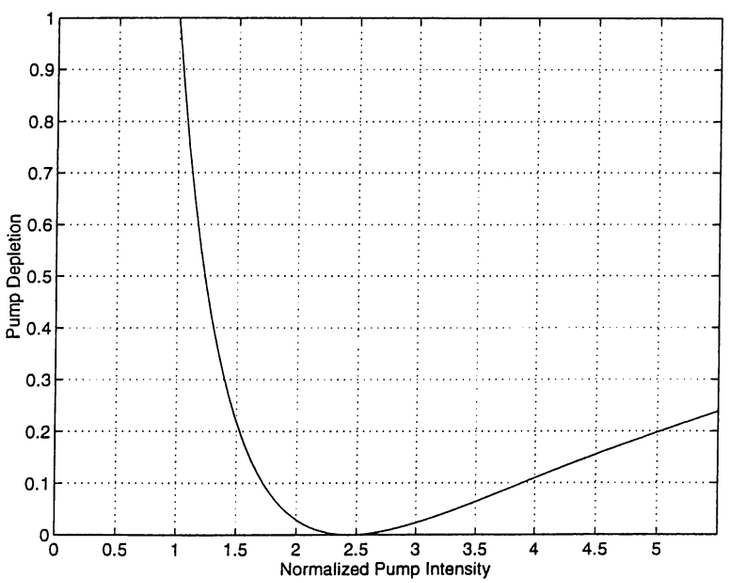

Figure 2.10: Pump depletion as a function of the normalized pump intensity to the threshold.

the pump intensity is fully depleted. Figure 2.10 shows the pump depletion $I_p(z = L)/I_p(z = 0)$ as a function of the normalized pump intensity to the threshold. The pump field can be fully depleted in the plane wave theory.

Chapter 3

Experimental Work

Optical parametric oscillators (OPO) are tunable sources of coherent radiation. They extend the wavelength range of conventional laser sources through down-conversion to longer wavelengths [5]. Development of the Kerr-lens mode-locked Titanium:Sapphire (Ti:Al_2O_3) laser has provided an excellent source to pump ultrafast OPOs. These lasers typically produce 100 fs pulses at a repetition rate on the order of 100MHz, with average powers greater than 1 W (corresponding to peak powers greater than 100 kW) and tunability between 700 and 1000 nm [13]. Many optical parametric oscillators have been demonstrated with ultrafast Ti:Sapphire lasers [11–16].

In this work, we investigate OPOs that are pumped by an ultrafast Ti:Sapphire laser. In Sections 3.1 and 3.2, properties of the laser source and the nonlinear crystal used in our experiment are outlined. The design of the oscillator cavity is discussed in Section 3.3. Non-ideal effects that we must take into account are described in Section 3.4. Results of our OPO experiment are given next. In the last section, we describe and give results of self-doubling OPO experiment.

A simple schematic of the OPO view is given in Figure 3.1. We use a Ti:Sapphire laser as our pump source. The output of the laser is tuned to a wavelength of 745 nm in the infrared. An 8 mm thick potassium titanyl phosphate ($KTiOPO_4$, KTP) crystal is employed as the nonlinear gain medium in the OPO. The KTP crystal is cut at $\theta = 90°$ and $\phi = 23°$, which results in a signal wavelength at 1068 nm.

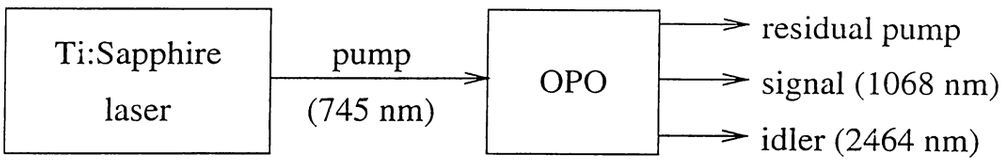

Figure 3.1: Schematic view of our OPO experiment.

3.1 The Laser

A mode-locked Ti:Sapphire laser (Coherent, Mira-900F) is used in our experiments. The laser is a tunable laser with a tuning range between 700 and 1000 nm. It has a pulse repetition rate of 76 MHz corresponding to the separation of the longitudinal modes of the laser. Kerr-lens mode-locking is employed to achieve nearly transform limited pulses of approximately 120 fs.

We operate at a wavelength of 745 nm. At this wavelength, the output of the laser is 640 mW resulting in an instantaneous peak power of 60 kW. We measure the duration of our laser pulses with an autocorrelator (Femtochrome FR103XL). At this wavelength, we measured the autocorrelation of our pulses to be 180 fs. When deconvolved assuming a hyperbolic secant pulse shape, the pulse duration is deduced to be 120 fs.

3.2 Potassium Titanyl Phosphate Crystal

Potassium titanyl phosphate ($KTiOPO_4$) is an $mm2$ point group, positive biaxial crystal whose transparency range is between 0.35–4.5 μm [17]. Sellmeier equations describing the dispersion relations for the principle-axis refractive indices n_x, n_y and n_z can be written as [17]

$$n_x^2 = 2.1146 + \frac{0.89188\lambda^2}{\lambda^2 - 0.043518132} - 0.0132\lambda^2 \tag{3.1}$$

$$n_y^2 = 2.1518 + \frac{0.87862\lambda^2}{\lambda^2 - 0.04752836} - 0.01327\lambda^2 \tag{3.2}$$

$$n_z^2 = 2.3136 + \frac{1.00012\lambda^2}{\lambda^2 - 0.056791656} - 0.01679\lambda^2 \tag{3.3}$$

Figure 3.2 shows the principle refractive indices for the KTP crystal.

The KTP crystal that we use is cut at $\theta = 90°$ and $\phi = 23°$. Its dimensions are $6 \times 6 \times 8$ mm. It is anti-reflection coated for 1064 nm on both faces. We use

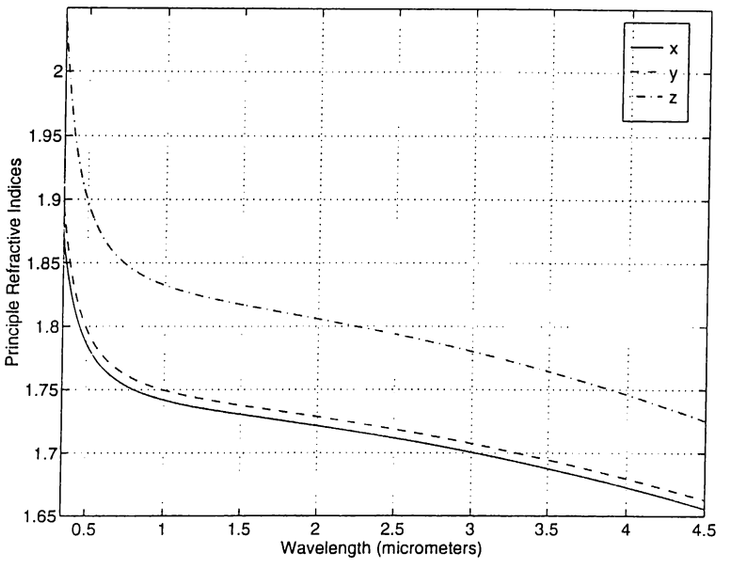

Figure 3.2: Principle refractive indices of KTP crystal.

a type-II phase matching geometry. The signal and pump fields are both p-polarized (horizontal, fast crystal axis), and the idler is s-polarized (vertical). Figures 3.3 and 3.4 are the phase matched wavelengths of signal and idler fields as a function of the wavelength of the pump field. The phase matched wavelengths of the idler and the signal are also marked at a pump wavelength of 745 nm. (See Appendix B for the details of phase matching.)

The effective nonlinear coefficient at any θ and ϕ angle can be calculated

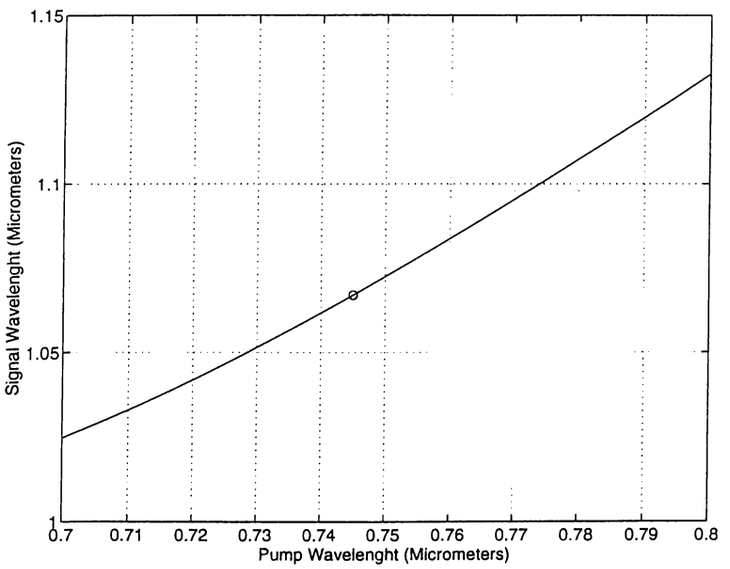

Figure 3.3: Phase matched signal wavelengths at crystal angles $\theta = 90°$ and $\phi = 23°$.

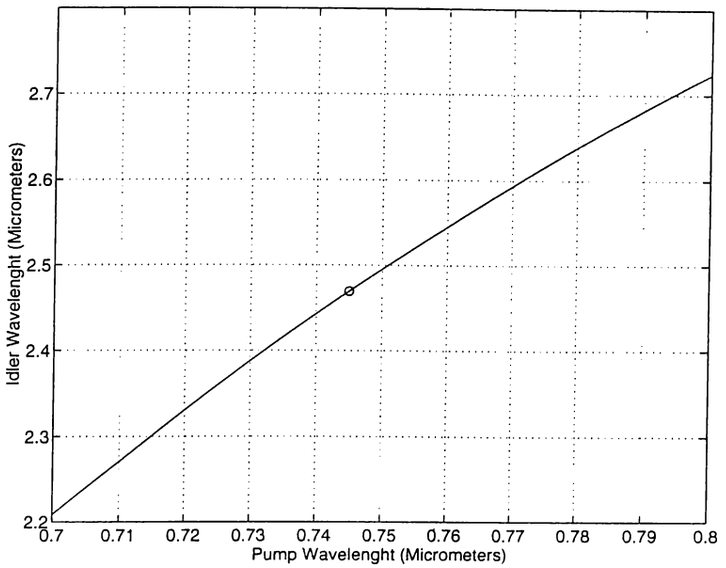

Figure 3.4: Phase matched idler wavelengths at crystal angles $\theta = 90°$ and $\phi = 23°$.

using Equation (2.28). The nonlinear coefficient is calculated to be [17]

$$d_{\text{eff}} = d_{15} \sin^2 \varphi + d_{24} \cos^2 \varphi \tag{3.4}$$

in the xy plane. For the KTP crystal, d_{15} and d_{24} are [18]

$$d_{15} = \frac{1}{2}\chi_{xxz} = 2.0 \times 10^{-12}\,\text{m/V} \tag{3.5}$$

$$d_{24} = \frac{1}{2}\chi_{yyz} = 3.6 \times 10^{-12}\,\text{m/V} \tag{3.6}$$

With $\varphi = 23°$,

$$d_{\text{eff}} = 3.4 \times 10^{-12}\text{m/V} \tag{3.7}$$

is found.

3.3 OPO Cavity

Figure 3.5 shows the experimental setup in detail. A ring cavity is formed by four mirrors. The signal light oscillates among the mirrors M1, M2, M3, and M4. M1 is a concave mirror with a radius of curvature of 10 cm. It is a high reflector for the signal as well as having high transmission coatings for the pump. M2 is an another concave mirror used to form a cavity focus between M1 and M2. It has a radius of curvature of 15 cm. It is also a high reflector for

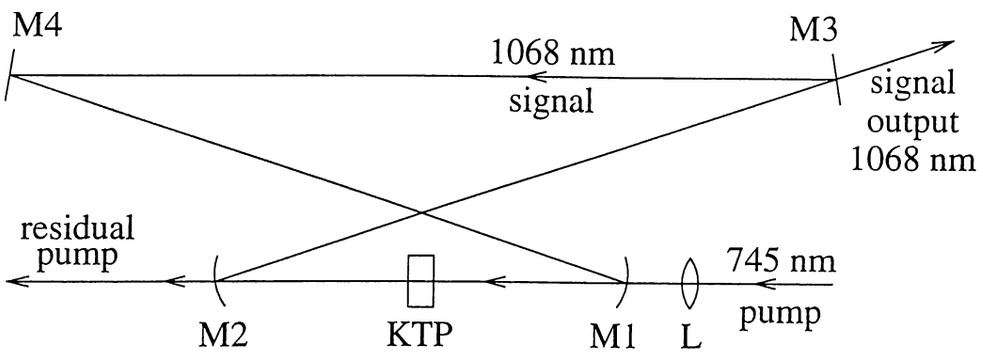

Figure 3.5: Experimental setup.

the signal with high transmission coatings for the pump and the idler. M3 and M4 are flat mirrors. M4 is a high reflector. M3 is used as an output coupler for the signal output. The mode-locked Ti:Sapphire laser provides the pump beam to the OPO at a wavelength of 745 nm. The pump beam is focused with a lens (L) of focal length 100 mm to match the intracavity focus and enters the cavity through M1. The KTP crystal is positioned at the intracavity focus. The mode radius supported by the cavity is calculated to be 20 μm, and the focused pump beam diameter is calculated to be 36 μm at the KTP crystal.

In the OPO, a pump pulse passes through the crystal once, providing gain for a signal pulse. The signal pulse propagates inside the cavity and reaches the crystal. If the signal pulse reaches at the same time with the pump pulse, it is amplified and the oscillation starts. Therefore, the cavity length is very important in these experiments. Changing the cavity length by moving M4,

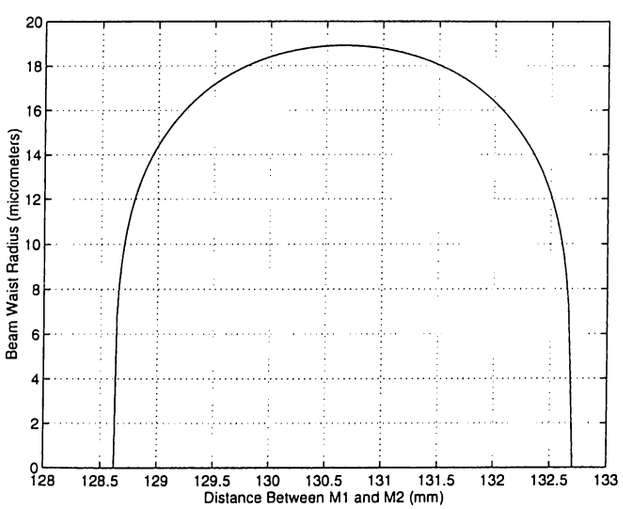

Figure 3.6: The cavity focus size (beam waist radius of signal light at focus) and stability range for distance between mirrors M1 and M2.

we can adjust the arrival time of the signal pulse to the crystal and make the signal pulse in synchronism with the repetition rate of the pump pulses. This pumping scheme is called synchronous pumping.

With the repetition rate r of the laser and the refractive index n of the crystal for the signal, and crystal length L, the cavity round trip length l_c must be

$$l_c = c_0/r - L(n-1) \tag{3.8}$$

for synchronization. In addition to this, the distance between the mirrors determines the stability of the cavity. Figure 3.6 shows the beam waist radius at the focus as a function of the distance between M1 and M2 with the cavity length l_c held constant. For a small range of distance, there is a stable region where the cavity is stable and a beam waist exists. To adjust the cavity properly, M2 is positioned on a translation stage for adjusting the distance between M1 and M2, so we use two translation stages for the adjustment of cavity.

3.4 Non-ideal Effects

The use of plane waves to model our experiment is a first order approximation. Most lasers generate beams that show a Gaussian distribution in the transverse direction. The pulse shape of pulsed lasers is also important.

The parametric gain is an intensity depended quantity. Due to the Gaussian intensity profile of the pump beam, the gain varies with the radial distance from the center. This non uniform distribution affects the conversion such that when one part of the pump beam is depleted the other parts are not. This lowers the conversion efficiency [19].

A similar concept is also valid for the pulse shapes, the intensity of the pulse is much higher in the middle than the tails, resulting in higher parametric gain there.

Other non-ideal effects come from the use of ultrashort pulses. A 100 fs pulse has a spatial extent of 30 μm. Due to material dispersion, the pump, signal, and idler pulses travel with different group velocities inside the crystal. As a result, the interaction length of the pulses is restricted by the overlap distance [20].

In dispersive media, the group velocity of pulses propagating at λ_0 can be

written as [21]

$$v = \frac{c}{N} \tag{3.9}$$

where

$$N = n - \lambda_0 \frac{dn}{d\lambda}\bigg|_{\lambda=\lambda_0} \tag{3.10}$$

where $n(\lambda)$ gives the wavelength dependence of the refractive index. The group velocity mismatch (GVM) is defined to be

$$\delta v_g^{-1} = \frac{1}{v_i} - \frac{1}{v_j} \tag{3.11}$$

where i and j represents pump, signal, and idler. At our operation wavelengths, the GVM between the pump and the signal pulses are calculated to be 126 fs/mm.

The effect of GVM is taken into account by introducing an effective length of interaction. Although the crystal length is 8 mm in our case, the length in which the pulses overlap is much less than this. For the calculation of threshold powers, we assume the initial signal pulse width is equal to the pump pulse width, because the first pulse is purely generated from the pump pulse. While these pulses travel, they go apart and the interaction ends when the pulses are separated from each other by 120 fs. The effective length is calculated to be

$$\frac{120\,\text{fs}}{126\,\text{fs/mm}} = 0.95\,\text{mm} \tag{3.12}$$

which is eight times smaller than the actual crystal length.

3.5 Measurements and Results

We made three types of measurements to characterize our OPOs, namely average power, pulse width, and spectral width. Power measurements give information about the conversion efficiency, whereas the pulse and spectral widths give information about the pulse quality.

The input pump power is measured before the focusing lens (L) (see Figure 3.5). A power divider (polarizer waveplate combination) is employed before the lens to adjust the input power. We take the signal output from M3. The signal power is measured after separating the signal beam from the residual pump beam using a prism. The prism is a Brewster angle prism and fully transmits the signal beam. Pump depletion is measured after M2. We measure the

Specified reflectance	Measured reflectance
98%	98.7%
95%	93.3%
90%	90.6%
87%	85.5%

Table 3.1: Output Coupler Reflectances.

remaining pump beam when the cavity is blocked (no oscillation) and when there is oscillation. The ratio shows us how much the pump beam is depleted in the interaction. The idler beam also leaves the cavity from M2. Therefore in this measurement, we actually measure the power of the depleted pump and the generated idler beam when cavity oscillates. As a result, our pump depletion measurements are not accurate, and underestimate the amount of depletion.

We use four different output coupler mirrors. In Table 3.1, the reflectivities of the output couplers are given. First column contains the specified values and the second column contains values that we measured. We obtain highest output power with the 10% output coupler. Figures 3.10 through 3.18 show the output power, the conversion efficiency, and the pump depletion, for the output couplers listed, as a function pump power.

The output power characteristics show an increase with increasing pump power, but this increase is not linear. When we look at the conversion efficiency curves, the conversion efficiency increases rapidly for pump powers just above the threshold, then reaches a saturation. We get maximum conversion of 170 mW corresponding to 27% conversion efficiency with the 10% output coupler. We compare the conversion efficiency curve for the 10% output coupler with a theoretical curve based on the plane wave theory (see Figure 3.7). Our experimental measurements are not close to what the plane wave theory predicts. The plane wave theory predicts 69% maximum conversion efficiency whereas we get 27% conversion efficiency. Also, the pump power at which the maximuin conversion is achieved are not the same. Similar statements also true for the pump depletion. Plane wave theory predicts that the pump can be fully depleted, but in the experiment, we can deplete it only by 44% (see Figure 3.8). This result is due to the Gaussian distribution of the beams. A calculation done by Bjorkholm [19] shows that 71% maximum pump depletion can be achieved for which the plane wave theory predicts 100% depletion. Bjorkholm, also, reported that the pump powers at which the maximum depletion occurs is larger than the plane wave case.

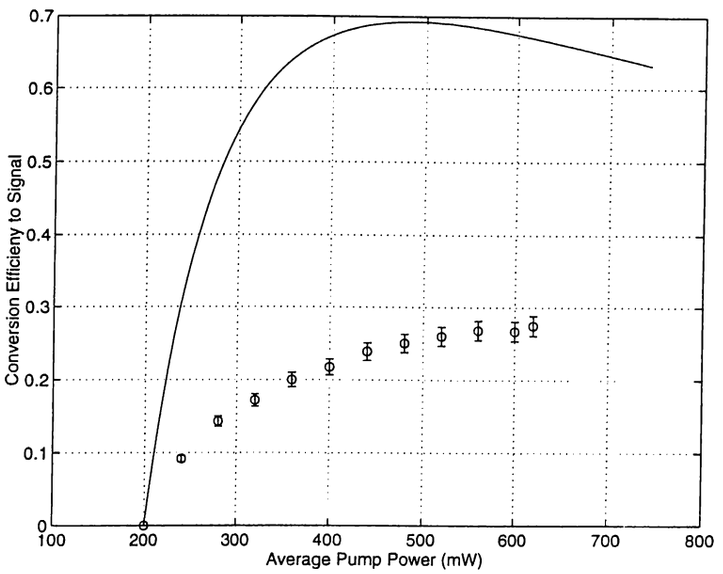

Figure 3.7: Conversion efficiency for the 90% output couple with the theoretical plane wave curve.

We expect the pump depletion to be maximum for the 10% output coupler, but we observe that it is maximum with the 2% percent output coupler. This indicates that the useless cavity losses are comparable with losses of the output couplers.

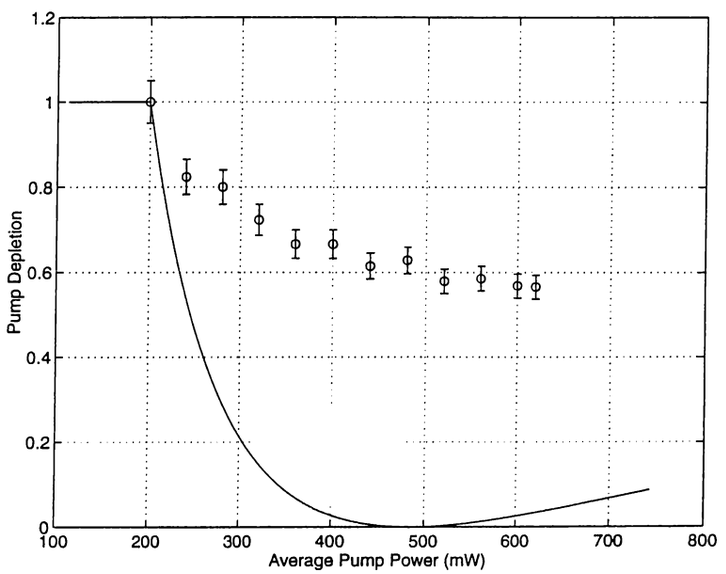

Figure 3.8: Pump depletion for the 90% output couple with the theoretical plane wave curve.

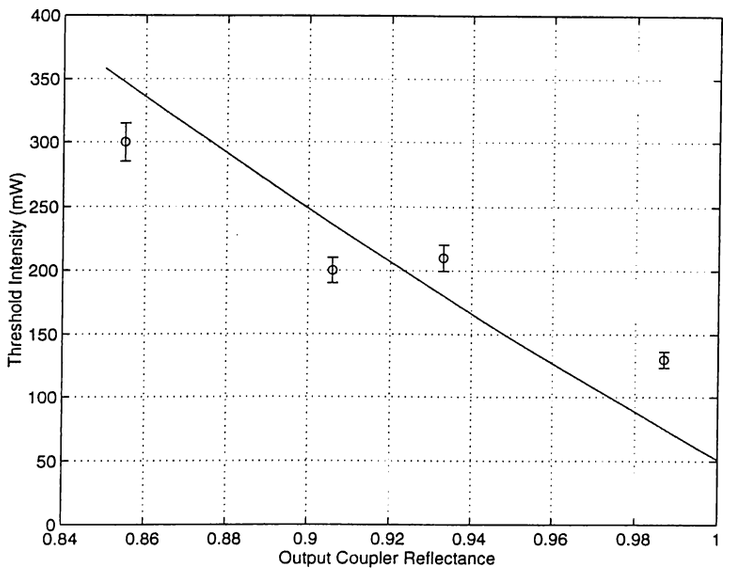

Figure 3.9: The threshold powers with respect to output coupler reflectances.

An approximate calculation of threshold powers can be done using plane wave theory. In these calculations, we assume that the pulses are square pulses having the same energy as the original pulses. The pulse width of these pulses are equal to the full width at half maximum of the original pulses. Also, we assume a uniform intensity distribution in the transverse plane. The full power is uniformly distributed inside a circular area with a radius that is equal to the beam waist radius. Then, we can estimate an average power from plane wave intensity by

$$I_{\mathrm{TH}} = \frac{P_{\mathrm{TH}}}{76\mathrm{MHz} \times 120\mathrm{fs} \times \pi \times W_0^2} \tag{3.13}$$

where W_0 is the beam waist radius, 120 fs is the full width at half maximum pulse width, and 76 MHz is the repetition rate of the pump pulse.

Figure 3.9 shows the threshold data as a function of output coupler reflectances . A plane wave theory curve is also given. The curve is calculated using Equation (2.89) with the lumped-loss reflectance of 97% and the effective length calculated using GVM. With that value of lumped losses the curve is

Specified reflectance	Auto-correlation width	Spectral with
98%	1181 fs	26 nm
95%	702 fs	31 nm
90%	651 fs	30 nm
87%	536 fs	24 nm

Table 3.2: Pulse and spectral widths.

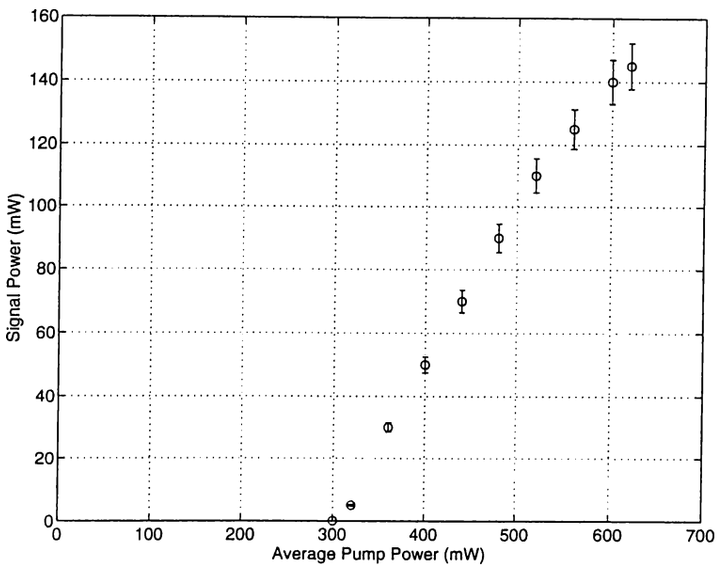

Figure 3.10: Average signal power for the 87% output coupler.

a best fit curve. Although the data points are not exactly on the curve, the general tendency is very similar.

Table 3.2 lists the spectral and autocorrelation widths of the signal field. Wide spectra and pulse widths compared to the pump pulses (120 fs pulse and 8.5 nm spectral widths) indicate that there are mechanisms that broaden the signal pulse duration and spectral width. At maximum conversion, the autocorrelation pulse width is 650 fs.

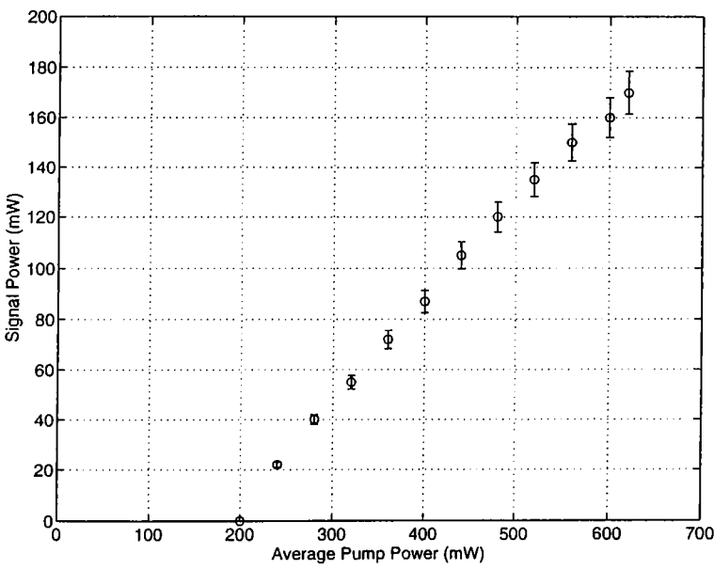

Figure 3.11: Average signal power for the 90% output coupler.

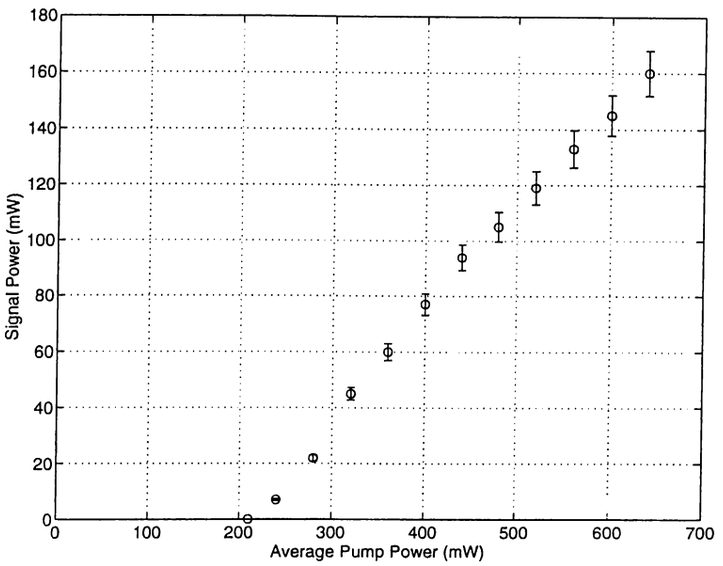

Figure 3.12: Average signal power for the 95% output coupler.

When we compare our OPO system with other Ti:Sapphire pumped OPO systems, our system has less efficiency and has longer pulse widths. In [22], a KTP based Ti:Sapphire laser pumped femtosecond OPO with the intracavity pulse compression is reported. The OPO has a 680 mW signal output at a wavelength of 1.3 μm with a pulse width of 115 fs when OPO pumped by a 2.4 W pump beam at a wavelength of 780 nm. The conversion efficiency is 28.3%. Our OPO has 27% conversion efficiency. Also the pulse width of our signal beam is much larger.

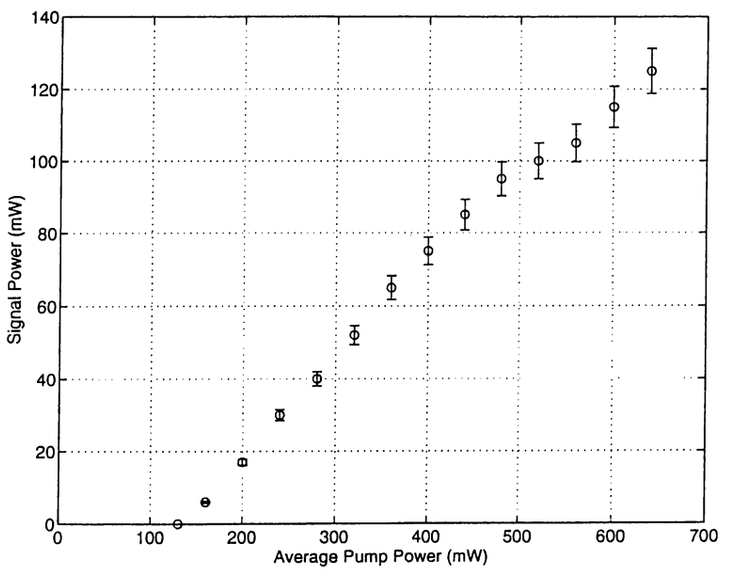

Figure 3.13: Average signal power for the 98% output coupler.

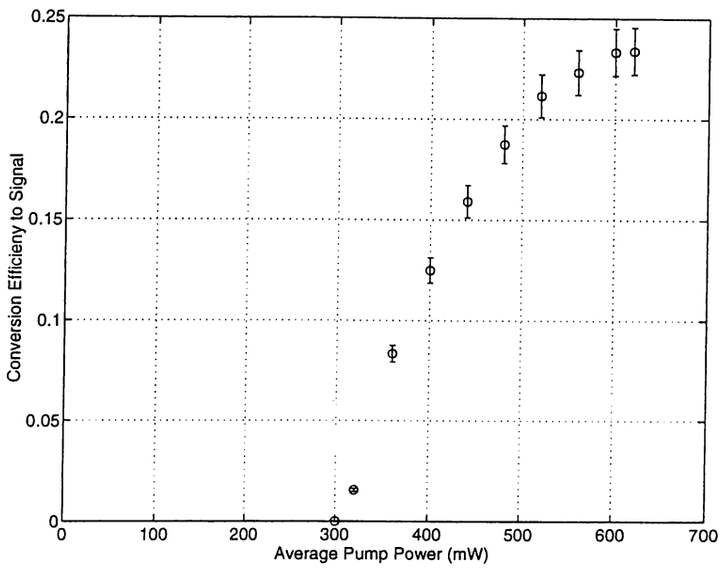

Figure 3.14: Conversion efficiency for the 87% output coupler

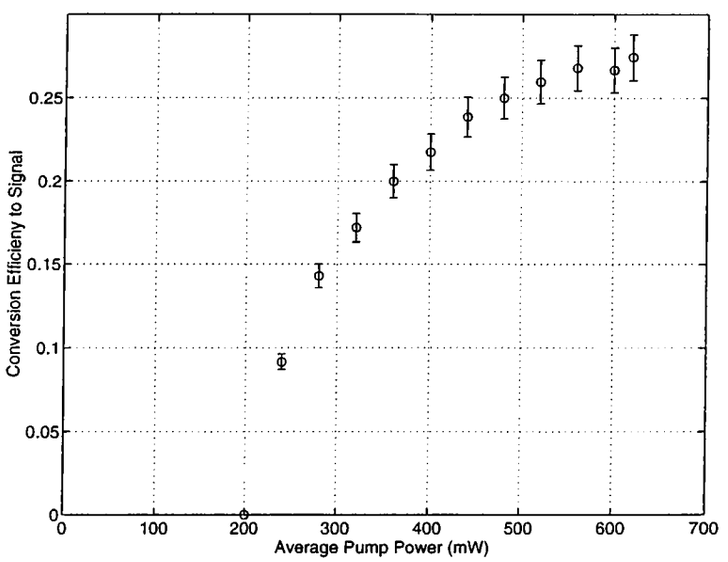

Figure 3.15: Conversion efficiency for the 90% output coupler.

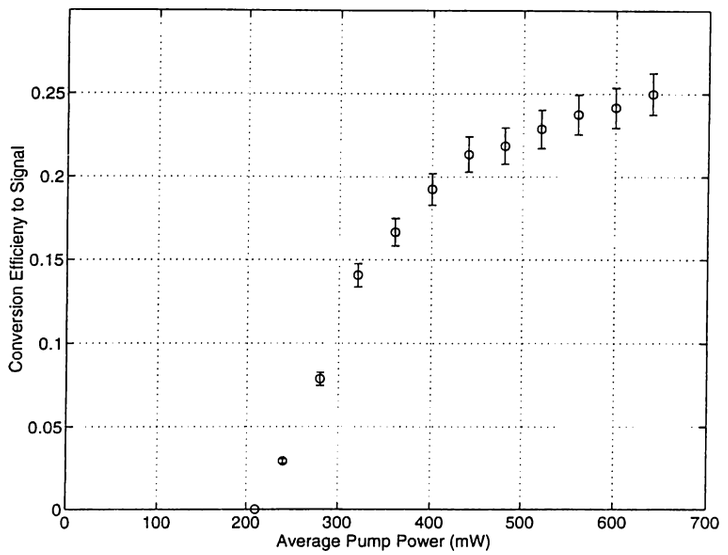

Figure 3.16: Conversion efficiency for the 95% output coupler.

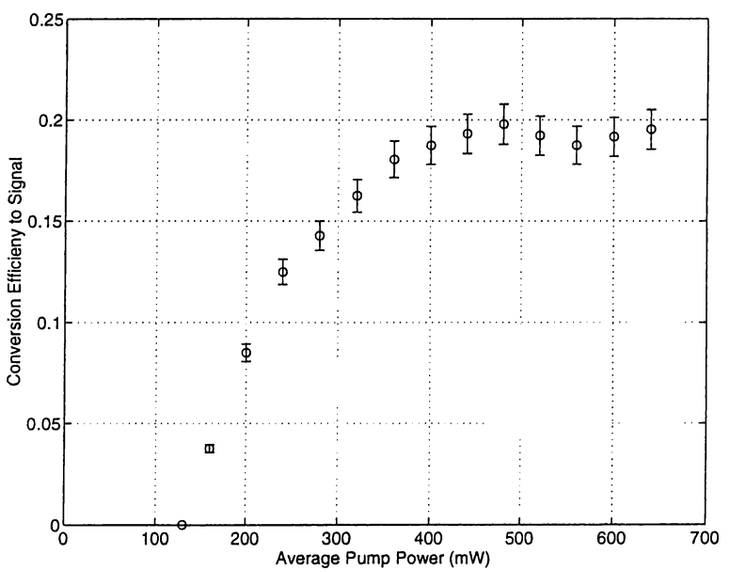

Figure 3.17: Conversion efficiency for the 98% output coupler.

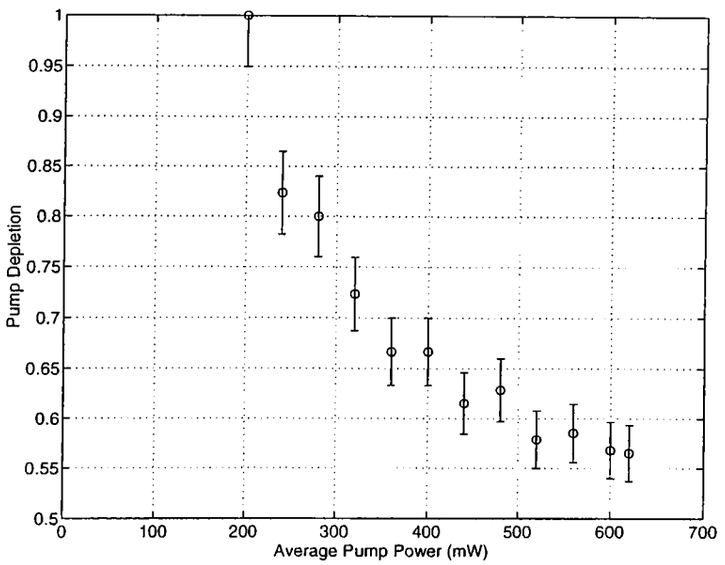

Figure 3.18: Pump depletion for the 90% output coupler.

3.6 Self Doubling OPO

Intracavity second harmonic generation is a technique used for frequency up-conversion [22–24]. A second crystal is placed inside the OPO cavity where the output coupler is replaced by a high reflector. The high intra cavity signal intensity is used for efficient frequency doubling. The second harmonic generation process acts as the output coupler of the OPO.

We have invented a new intracavity frequency doubling scheme that uses a single crystal for both parametric generation and frequency doubling [25].

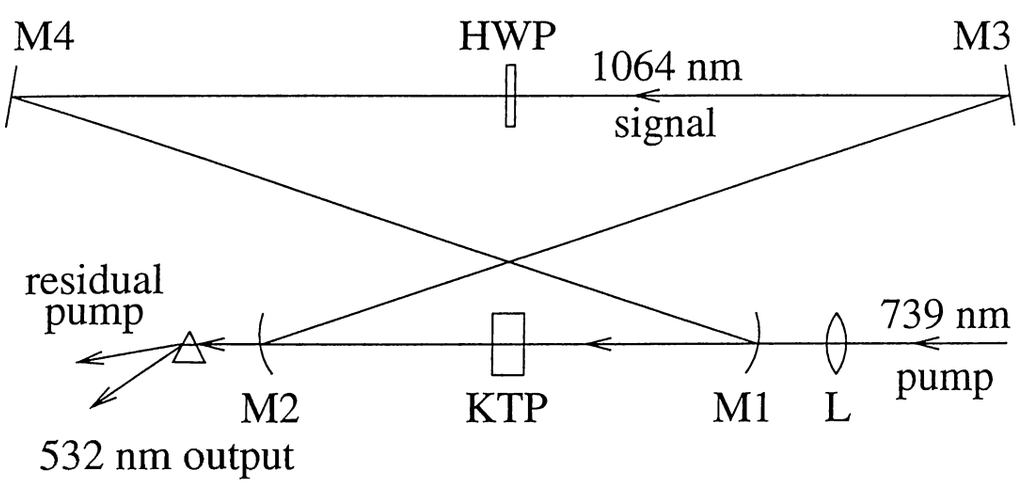

Figure 3.19: Self-doubling OPO setup.

The experimental setup is very similar to the regular OPO experiment. Our self-doubling OPO is pumped by a Ti:Sapphire laser operating at a wavelength of 739 nm. As a result, the signal wavelength of the OPO is at 1064 nm, corresponding to an idler wavelength of 2420 nm. The OPO cavity resonates only the signal wavelength. The signal beam is also phase-matched for second harmonic generation (SHG) at the same crystal orientation. With proper polarization rotation, an output beam at a wavelength of 532 nm can be obtained. To the best of our knowledge, this is the first demonstration of optical parametric oscillation and phase-matched frequency doubling within a single crystal.

We use the same 8 mm long KTP crystal cut for doubling 1064 nm in a type-II phase-matching geometry ($\theta = 90°, \phi = 23°$). The crystal has antireflection coatings for the fundamental and second-harmonic wavelengths. The second-harmonic output is p-polarized. In parametric generation, the pump at 739 nm and the signal at 1064 nm are both p-polarized, and the idler at 2420 nm is s-polarized.

A ring cavity is made of four mirrors that are high reflectors at 1064 nm as shown in Figure 3.19. M1 and M2 are 25 cm radius concave, M3 is a 3 m radius concave, and M4 is a flat mirror. The KTP crystal is positioned at the intracavity focus between M1 and M2. The pump beam is focused with a lens (L) of focal length 15 cm and enters into the cavity through M1. For efficient frequency doubling, a half-wave retarder at 1064 nm is placed inside the OPO cavity which couples some of the horizontally polarized signal beam

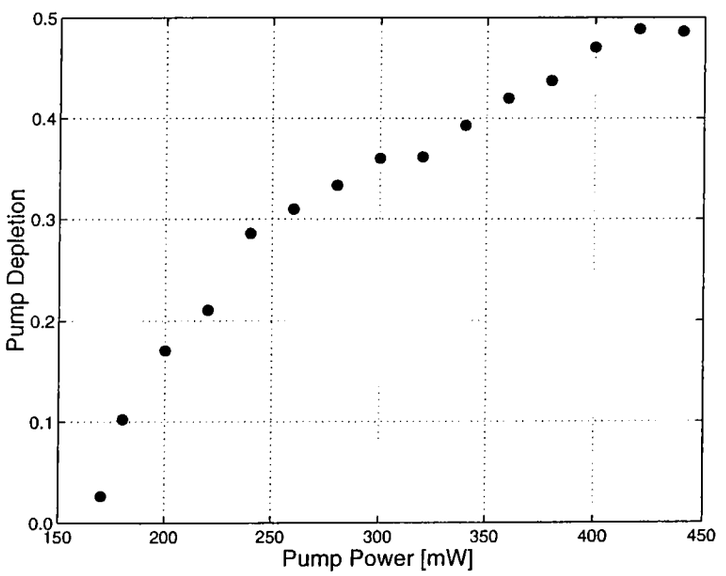

Figure 3.20: Pump depletion as a function of pump power.

to the vertical. The length of the cavity is adjusted by moving M4 in order to synchronize the intracavity signal pulses with the pump pulses. The frequency doubled beam at 532 nm exits the cavity through M2. In addition, there is a weak 1064 nm beam coming out through M3, as this mirror has a slightly lower reflectance compared to the other cavity mirrors. This output is used to probe the signal beam for measurements.

When the half-wave retarder is not in the cavity, there is no (or very little) frequency doubling. This results in an undercoupled OPO cavity for the signal beam. We measured the threshold for this OPO to be 60 mW. At a pump power of 500 mW, the pump beam is depleted by more than 50%, showing strong conversion. In the case of frequency doubling with the retarder in place, the threshold of the OPO becomes 170 mW. At a pump power of 440 mW, 25 mW of 532 nm is obtained, corresponding to 6% conversion efficiency to the green. Figure 3.20 shows the pump depletion with the retarder in the cavity. Depletion is seen to be as high as before, indicating strong conversion to the signal wavelength.

Compared to intracavity SHG systems with another crystal [22, 23], our system is less efficient because it is not well optimized. Although our system works well, higher efficiencies can be reach by optimizing the cavity focus size, the focusing of pump beam and the length of the KTP crystal.

Chapter 4

Conclusion

This thesis outlines our experimental work to construct and characterize KTP crystal based ultrafast optical parametric oscillators. We use a femtosecond Titanium:Sapphire laser as a pump source at a wavelength of 745 nm. Our OPO converts this pump beam to a signal beam at a wavelength of 1068 nm.

We get a maximum signal intensity of 170 mW when the OPO is pumped with 640 mW and the 10% output coupler is used, corresponding to 27% conversion efficiency. The corresponding pump depletion is better than 44%. We need smaller cavity focii to reach higher signal intensities with higher output couplers.

We observe that the signal beam has larger spectral and pulse width than the pump beam. With the increase in output coupling, we get shorter pulses. Our future work includes the construction of dispersion compensation schemes to investigate the effects on pulse and spectral widths. Also, we plan to use different cavity mirrors and lenses to increase the focusing of the signal and pump beams for better conversion efficiency.

In addition, we have demonstrated a self-doubling OPO where the intracavity signal light at a wavelength of 1064 nm is doubled by the same KTP crystal. This is possible because our crystal is also phase matched for type-II second harmonic generation of at a wavelength of 1064 nm. For efficient conversion, we place a halfwave plate inside the cavity to rotate the polarization of the signal beam for the type-II phase matching geometry. To the best of our knowledge, this is the first demonstration of intracavity second harmonic generation with a single crystal used for both parametric oscillation and second

harmonic generation.

It is possible to find crystal angles that are phase matched for both optical parametric oscillation and sum frequency generation with the signal and pump beams. This self-summing OPO will be able to convert the pump to higher frequencies. Our long term aim is to investigate the single crystal intracavity second harmonic and sum frequency generation in more detail.

In this work, we only demonstrate a single operation wavelength. However, both OPOs are continuously tunable. We designed a self-doubling OPO which uses a non-critically phase-matched KTP crystal ($\theta = 90°$ and $\phi = 0°$). In this OPO, when the pump beam is at 744 nm, the OPO signal is at 1080 nm, and the doubled signal is at 540 nm. It is possible to tune this self-doubling OPO by changing the wavelength of the pump beam together with the crystal angles. Varying θ from 90° to 75° ($\phi = 0°$) and the pump wavelength from 744 nm to 750 nm, it is possible to generate frequency doubled output between 540 nm and 564 nm. Changing ϕ from 0° to 30° ($\theta = 90°$) and the pump wavelength from 745 nm to 739 nm, one can get 540 nm to 529 nm frequency doubled output. Our future work also includes the demonstration of the full tuning range of the newly designed self-doubling OPO for which we expect to get much better conversion efficiency.

In this thesis, we outline the plane wave theory of second-order nonlinear interactions. Although we explain the threshold powers with this theory, it is not suitable for power characteristics. The effects that are due to the Gaussian transverse profile of the pump, signal and idler beams and pulsed operation must be taken into account. We also plan to develop methods that are give precise predictions of OPO characteristics.

Appendix A

Optics of Crystals

The general constitutive relation of homogeneous, lossless and magnetically isotropic and inactive material for an arbitrary coordinate system is given as

$$\begin{bmatrix} D_{x'} \\ D_{y'} \\ D_{z'} \end{bmatrix} = \epsilon_0 \begin{bmatrix} \epsilon_{x'x'} & \epsilon_{x'y'} & \epsilon_{x'z'} \\ \epsilon_{x'y'} & \epsilon_{y'y'} & \epsilon_{y'z'} \\ \epsilon_{x'z'} & \epsilon_{y'z'} & \epsilon_{z'z'} \end{bmatrix} \begin{bmatrix} E_{x'} \\ E_{y'} \\ E_{z'} \end{bmatrix} = \epsilon_0 \bar{\epsilon} \cdot \begin{bmatrix} E_{x'} \\ E_{y'} \\ E_{z'} \end{bmatrix} \tag{A.1}$$

Each component of the electric displacement vector **D** is linearly related to the components of the electric field with the real elements of relative permittivity matrix. With the correct coordinate transformation, the real and symmetric relative permittivity matrix can be diagonalized for eigen-directions of x, y and z of a rectangular coordinate frame

$$\begin{bmatrix} D_x \\ D_y \\ D_z \end{bmatrix} = \epsilon_0 \begin{bmatrix} \epsilon_x & 0 & 0 \\ 0 & \epsilon_y & 0 \\ 0 & 0 & \epsilon_z \end{bmatrix} \begin{bmatrix} E_x \\ E_y \\ E_z \end{bmatrix}. \tag{A.2}$$

The diagonal components of relative permittivity matrix can be related to the refractive index of the corresponding eigen directions of axis as

$$\epsilon_i = n_i^2 \tag{A.3}$$

where $i = x, y, z$ and

$$n_x \leq n_y \leq n_z \tag{A.4}$$

by convention. For isotropic crystals, all three axial refractive indices are the same, so the constitutive relation can be expressed with a scalar instead of a

matrix

$$\mathbf{D} = \epsilon_0 \epsilon_r \mathbf{E}. \tag{A.5}$$

The refractive index is a constant for all polarization and propagation directions. The only dependence of the refractive index is to wavelength due to the dispersion. For anisotropic materials, either one or all of the three axial refractive indices are different. As a result, the refractive index seen by optical field depends on the polarization and propagation directions.

The Helmholtz wave equation

$$\mathbf{k} \times \mathbf{k} \times \mathbf{E} + \omega^2 \mu_0 \epsilon_0 \bar{\epsilon} \cdot \mathbf{E} = 0, \tag{A.6}$$

where $\mathbf{k}$, $\mathbf{E}$ and ω are the wave vector, electric field, and angular frequency, describes the propagation of plane waves inside the anisotropic material. The wave equation can be expressed as a matrix-vector product as

$$\left[k_0^2 \bar{\epsilon} + \mathbf{k}^{\mathbf{T}} \mathbf{k} - k^2 \bar{\mathbf{I}}\right] \cdot \mathbf{E} = 0. \tag{A.7}$$

This equation can be thought of as an eigen-value equation in k^2. Then the refractive index can be found to be $n = k/k_0$. There are two solutions of eigen-refractive indices exist. They gives two eigen polarization direction of the electric field.

The dispersion equation can be re-written in the form of quadratic equation in n^2 [26] as

$$\left(\hat{\mathbf{k}} \cdot \bar{\epsilon} \cdot \hat{\mathbf{k}}\right) n^4 + \hat{\mathbf{k}} \cdot \left[\text{adj}\, \bar{\epsilon} - \text{Tr}(\text{adj}\, \bar{\epsilon}) \bar{\mathbf{I}}\right] \cdot \hat{\mathbf{k}} n^2 + |\bar{\epsilon}| = 0 \tag{A.8}$$

where adj is the adjoint and Tr is the trace of the matrix. The two roots give the corresponding refractive indices as

$$A = \hat{\mathbf{k}} \cdot \bar{\epsilon} \cdot \hat{\mathbf{k}} = n_x^2 k_x^2 + n_y^2 k_y^2 + n_z^2 k_z^2 \tag{A.9}$$

$$\begin{aligned} B &= \hat{\mathbf{k}} \cdot \left[\text{adj}\, \bar{\epsilon} - \text{Tr}(\text{adj}\, \bar{\epsilon}) \bar{\mathbf{I}}\right] \cdot \hat{\mathbf{k}} = \\ &= -n_y^2 n_z^2 \left(1 - k_x^2\right) - n_x^2 n_z^2 \left(1 - k_y^2\right) - n_x^2 n_y^2 \left(1 - k_z^2\right) \end{aligned} \tag{A.10}$$

$$C = |\bar{\epsilon}| = n_x^2 n_y^2 n_z^2 \tag{A.11}$$

$$n = |\mathbf{k}| / k_0 \tag{A.12}$$

$$n_{1,2}^2 = \frac{-B \mp \left(B^2 - 4AC\right)^{1/2}}{2A} \tag{A.13}$$

The eigen polarization directions of the electric field are also important for the calculations of the nonlinear coefficient d_{eff} (see Equation (2.28)). A vector in the direction of electric field can be easily found by

$$\mathbf{e}_{1,2} = \text{adj}\, W(\hat{\mathbf{k}}, n_{1,2}) \cdot \mathbf{c} \tag{A.14}$$

$$W(\hat{\mathbf{k}}, n) = \bar{\epsilon} + n^2(\hat{\mathbf{k}}^{\mathbf{T}}\hat{\mathbf{k}} - \bar{\mathbf{I}}) \tag{A.15}$$

where $\mathbf{c}^T = [\ 1 \quad 1 \quad 1\ ]$ [27].

Appendix B

Phase Matching

In Section 2.3, it is stated that the nonlinear effect is less efficient for nonzero Δk in three wave mixing. To achieve $\Delta k = 0$, the equations

$$n_1\omega_1 + n_2\omega_2 = n_3\omega_3 \tag{B.1}$$

$$\omega_1 + \omega_2 = \omega_3 \tag{B.2}$$

have to be satisfied simultaneously. For isotropic crystals this is impossible. The most common way to achieve phase matching is to use birefringent crystals for which the refractive index is dependent on the polarization and the direction of propagation of optical field.

There are two eigen-refractive indices for the propagation in a birefringent crystal. One of them is always less than or equal to other resulting faster phase velocity. We name them as the fast and the slow refractive indices.

In order to achieve phase-matching, the highest frequency wave ω_3 is polarized in the direction that gives it fast refractive index. There are two choices for the polarizations of the lower-frequency waves [28]. If the waves at frequencies ω_1 and ω_2 have the same polarization which is orthogonal to the polarization of the wave at frequency ω_3, this is called type-I phase-matching. For type-II phase matching, the waves at frequencies ω_1 and ω_2 have orthogonal polarizations and one of them has the same polarization with the highest frequency wave ω_3. Figure B.1 shows the directions of polarization of the waves in type-I and type-II phase matching.

We have two phase matching problems that we want to solve. One of them is to find a propagation direction for a known frequency of the pump beam

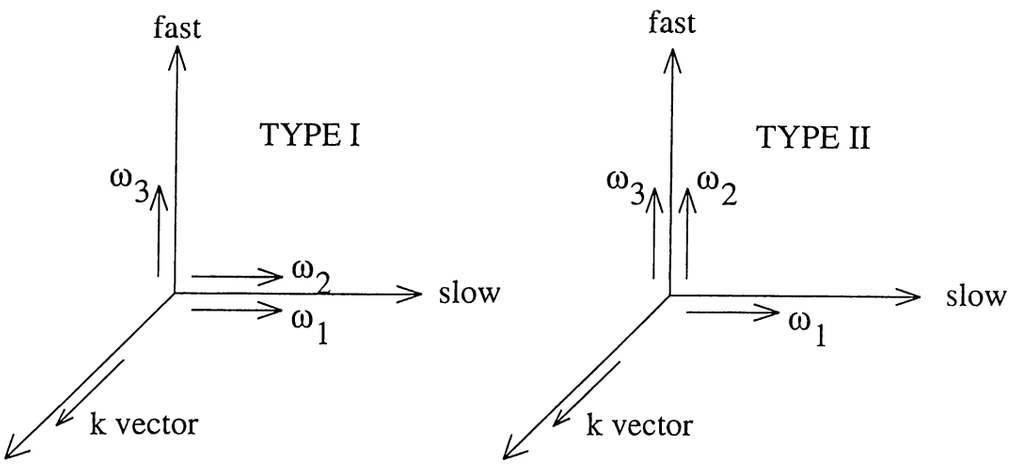

Figure B.1: Directions of polarizations for ω_1, ω_2, and ω_3 for type-I and type-II phase matching in three wave mixing ($\omega_1 + \omega_2 = \omega_3$).

and desired operation frequency of the signal beam. The other problem is to find the signal frequency of operation for a given direction of propagation with a known frequency of the pump beam. With the type information, the phase matching equation takes the form for type-I interact as

$$n_f(\omega_3, \theta, \phi)\omega_3 = n_s(\omega_1, \theta, \phi)\omega_1 + n_s(\omega_2, \theta, \phi)\omega_2 \tag{B.3}$$

where θ and ϕ angles are spherical angles specifying the direction of propagation in rectangular coordinate frame of xyz. The corresponding equation for type-II phase matching is

$$n_f(\omega_3, \theta, \phi)\omega_3 = n_f(\omega_1, \theta, \phi)\omega_1 + n_s(\omega_2, \theta, \phi)\omega_2. \tag{B.4}$$

With the frequency condition $\omega_3 = \omega_1 + \omega_2$, phase matching equations can be solved numerically.

The wavelength dependence of the refractive indices are given by the Sellmeier equations for the principle axis refractive indices. The calculations of the eigen refractive indices and eigen-polarizations are given in Appendix A.

REFERENCES

[1] T. H. Maiman, *Nature*, vol. 187, p. 493, 1960.

[2] P. A. Franken, A. E. Hill, C. W. Peters, and G. Weinreich, "Generation of optical harmonics," *Physical Review Letters* , vol. 7, pp. 118-119, 1961.

[3] N. Kroll, "Parametric amplification in spatially extended media and application to the design of tunable oscillators at optical frequencies," *Physical Review*, vol. 127, p. 1207, 1962.

[4] J. A. Giordimane and R. C. Miller, "Tunable coherent parametric oscillation in $LiNbO_3$ at optical frequencies," *Physical Review Letters*, vol. 14, pp. 973-976, 1965.

[5] Special issue on Optical Parametric Oscillators and Amplifiers, *Journal of the Optical Society of America Part B*, vol. 10, pp. 1656-2243, 1993.

[6] D. C. Edelstein, E. S. Wachman, and C. L. Tang, "Broadly tunable high repetition rate femtosecond optical parametric oscillator," *Applied Physics Letters*, vol. 54, p. 1728, 1989.

[7] R. W. Boyd, *Nonlinear Optics.* Academic Press, Inc., San Diego, 1992.

[8] D. K. Cheng, *Field and Wave Electromagnetics.* Addison-Wesley, 1991.

[9] R. A. Baumgartner, and R. L. Byer, "Optical parametric amplification," *IEEE Journal of Quantum Electronics*, vol QE-15, pp. 431-445, 1979.

[10] D. F. Lawden, *Elliptic Functions and Applications.* Springer-Verlag, New York, 1989.

[11] A. Nebel, C. Fallnich, R. Beigang, and R. Wallenstein, "Noncritically phase-matched continuous-wave mode-locked singly resonant optical parametric oscillator synchronously pumped by a Ti:sapphire laser," *Journal of the Optical Society of America Part B*, vol. 10, pp. 2195-2200, 1993.

[12] H. H. Zenzie and P. F. Moulton, "Tunable optical parametric oscillators pumped by Ti:sapphire laser," *Optics Letters*, vol. 19, no. 13,pp. 963-965, 1994.

[13] Q. Fu, G. Mak, and H. M. van Driel, "High-power, 62-fs infrared optical parametric oscillator synchronously pumped by a 76-MHz Ti:sapphire laser," *Optics Letters*, vol.17,pp. 1006-1008, 1992.

[14] R. J. Ellingson, and C. L. Tang, "High-power, high-repetition-rate femtosecond pulses tunable in the visible," *Optics Letters*, vol. 18, no. 6, pp. 438-440, 1993.

[15] P. E. Powers, R. J. Ellingson, W. S. Pelouch and C. L. Tang, " Recent advances of the Ti:sapphire-pumped high-repetition-rate femtosecond optical parametric oscillator," *Journal of the Optical Society of America Part B*, vol. 10, pp. 2162-2167, 1993.

[16] J. M. Dudley, D. T. Reid, M. Ebrahimzadeh, and W. Sibbett, "Characteristics of a Noncritically phase-matched Ti:sapphire pumped femtosecond optical parametric oscillator," *Optics Communication*, vol. 104, no. 4,5,6, pp. 419-430, 1994.

[17] V. G. Dimitriev, G. G. Gurzadyan, and D. N. Nikogosyan, *Handbook of Nonlinear Optical Crystals*, Springer-Verlag, Berlin, 1991.

[18] D. A. Roberts, "Simplified characterization of uniaxial and biaxial nonlinear optical crystals: a plea for standardization of nomenclature and conventions," *IEEE Journal of Quantum Electronics*, vol. QE-28, pp. 2057-2074, 1992.

[19] J. E. Bjorkholm, "Some effects of spatially nonuniform pumping in pulsed optical parametric oscillators," *IEEE Journal of Quantum Electronics*, vol. QE-7, pp. 109-118, 1971.

[20] D. T. Reid, M. Ebrahimzadeh, and W. Sibbett, "Design criteria and comparison of femtosecond optical parametric oscillators based on $KTiOPO_4$ and $RbTiOAsO_4$," *Journal of the Optical Society of America Part B*, vol. 12, pp. 2168-2179, 1995.

[21] B. E. A. Saleh, M. C. Teich. *Fundamentals of Photonics.* John Wiley and Sons Inc., New York, 1991.

[22] P. E. Powers, R. J. Ellingson, W. S. Pelouch, and C. L. Tang, "Recent advances of Ti:Sapphire-pumped high repetition rate femtosecond optical

parametric oscillator," *Journal of the Optical Society of America Part B*, vol. 10, pp. 2162-2166, 1993.

[23] R. J. Ellingson and C. L. Tang, "High-power, high-repetition-rate femtosecond pulses tunable in the visible," *Optics Letters*, vol. 18, pp. 438-440, 1993.

[24] L. R. Marshall, A. Kaz, and O. Aytür, "Continuously tunable diode-pumped UV-blue laser source," *Optics Letters*, vol. 18, pp. 817-819, 1993.

[25] T. Kartaloğlu, K. G. Köprülü, and Orhan Aytür, "Phase-Matched Self-Doubling Optical Parametric Oscillator," to be presented at *the Annual Meeting of IEEE Lasers and Electro-Optics Society*, Boston, Massachusetts, 18-22 November 1996.

[26] H. C. Chen, *Theory of Electromagnetic Waves A Coordinate-Free Approach*. McGraw-Hill, New York, 1985.

[27] T. A. Maldonado, T. K. Gaylord, "Light propagation characteristics for arbitrary wavevector directions in biaxial media by a coordinate-free approach," *Applied Optics*, vol. 30, pp. 2465-2480 , 1991.

[28] J. T. Wang and K. Daneshvar, "Numerical calculation of the effective second-order nonlinear coefficient along collinear phase-matching directions inside nonlinear crystal in three-wave interaction," *IEEE Journal of Quantum Electronics*, vol. 32, pp. 183-190, 1996.